16

NASA Contractor Report 165666

Boeing

Total Main Rotor Isolation System Analysis

V. Sankewitsch

Contract NAS1-16176

March 1981

National Aeronautics and Space Administration

Langley Research Center
Hampton, Virginia 23665

NASA Contractor Report 165666

Total Main Rotor Isolation System Analysis

V. Sankewitsch

BOEING VERTOL COMPANY
P. O. Box 16858
Philadelphia, Pa. 19142

Contract NAS1-16176

March 1981

National Aeronautics and
Space Administration

Langley Research Center
Hampton, Virginia 23665

TABLE OF CONTENTS

TABLE OF CONTENTS (Cont'd)

List of Figures

List of Tables

List of Symbols

Coordinates

x	Longitudinal displacement, m (in)
y	Lateral displacement, m (in)
z	Vertical displacement, m (in)
α	Roll rotation, radians
β	Pitch rotation, radians
γ	Yaw rotation, radians
δ	Spring deflection, m (in)

Subscripts - coordinate

X	Transmission
F	Fuselage
C	Cockpit (pilot's location)

Geometry

r	Distance from transmission pivot to fuselage pivot, m (in)
R	Distance from transmission pivot to inertia bar CG, m (in)
ℓ_x	Distance from transmission ℄ to transmission pivot on inertia bar, m (in)
ℓ_s	Distance from transmission ℄ to line of action of vertical and tangential IRIS springs, m (in)
θ	Angle between r/h fwd transmission leg and y-axis, degrees
R_r	R/r, pivot separation ratio
d	Vertical distance between XMSN CG and hub, m (in)
h_X	Vertical distance between mount plane and XMSN CG, m (in)
h_F	Vertical distance between fuselage CG and mount plane, m (in)
X_G	Longitudinal distance between XMSN CG and fuselage CG, m (in)

List of Symbols

Springs

K	Spring rate, N/m (lb/in)
K_v	IRIS vertical spring rate, N/m (lb/in)
K_τ	IRIS tangential spring rate, N/m (lb/in)
K_r	IRIS radial spring rate, N/m (lb/in)
K_p	Fuselage and transmission pivot bearing spring rate, N-m/rad (lb-in/rad)
K_s	Fuselage fitting bearing spring rate, N-m/rad (lb-in/rad)

Masses and Inertias

m	IRIS inertia bar mass, kg (lb-sec^2/in)
ρ	IRIS inertia bar radius of gyration about own CG, m (in)
M_X	Transmission mass, kg (lb-sec^2/in)
M_F	Fuselage mass, kg (lb-sec^2/in)
M_{IA}	Antiresonant IRIS mass = $[(R/r-1)R/r+(\rho/r)^2]$, kg (lb-sec^2/in)
M_{XX}	Effective transmission mass = $M_X+m[(R/r-1)^2+(\rho/r)^2]$, kg (lb-sec^2/in)
M_{FF}	Effective fuselage mass = $M_F+m[(R/r)^2+(\rho/r)^2]$, kg (lb-sec^2/in)
M_R	Coupled system modal mass, kg (lb-sec^2/in)
M_S	Mass ratio M_F/M_X
$k_{x\alpha}$	Transmission radius of gyration in roll, m (in)
$k_{x\beta}$	Transmission radius of gyration in pitch, m (in)
$k_{x\gamma}$	Transmission radius of gyration in yaw, m (in)
$k_{F\alpha}$	Fuselage radius of gyration in roll, m (in)
$k_{F\beta}$	Fuselage radius of gyration in pitch, m (in)
$k_{F\gamma}$	Fuselage radius of gyration in yaw, m (in)

List of Symbols

Damping

g	Structural damping constant in $F_{spring} = K(1+jg)\delta$, $j=\sqrt{-1}$
g_v	Structural damping in vertical and tangential IRIS springs
g_p	Structural damping in pivot gearings

Frequencies

ω	Forcing frequency, rad/sec
Ω	Rotor speed, rad/sec
ω_A	Antiresonant frequency, rad/sec
ω_R	Coupled system resonant frequency, rad/sec
η	ω/Ω forcing frequency ratio
N_R	Normal main rotor operating speed, RPM

Miscellaneous

n	Number of blades
E	Energy taken out of system by damping, N-m (lb-in)
G	Gravitational acceleration, 9.8 m/sec (386 in/sec)
$[A]$	Mass matrix
$[C]$	Stiffness matrix
$[L]_i$	Linear motion matrix for i^{th} IRIS bar
$[R]_i$	Angular motion matrix for i^{th} IRIS bar
$[D]_i$	Spring deflection matrix for i^{th} IRIS bar
$\{q\}$	Displacement vector
$\{F\}$	Force vector

1. Summary

This report documents the work performed by Boeing Vertol under NASA contract NAS1-16176. As stated in the contract, the objective of the study was to establish the requirements, preliminary design, and verification procedure for a total main rotor isolation system at n/rev. For the purpose of this effort, total main rotor isolation at n/rev is considered to be such that there is no n/rev response at any point on the fuselage due to main rotor shaft loads.

2. Introduction

A rotating blade experiences aerodynamic pressure loading which induces blade motion (see Figure 2.1a). Blade motion generates blade inertia loads (see Figure 2.1b) which modify the aerodynamic loads to yield blade root loads (see Figure 2.1c). The main rotor loads (see Figure 2.1d) represent the contribution of each individual blade, summed over all of the blades of the rotor at the same instant in time.

A rotor which is well balanced, both mechanically and aerodynamically, will transmit loads to the fuselage only at specific frequencies, namely multiples of the product of the main rotor speed, Ω, and the number of blades per rotor, n: $n\Omega$, $2n\Omega$, $3n\Omega$, etc. These $kn\Omega$ ($k = 1, 2, 3 \ldots$) fixed system loads have their origin at the same frequency ($kn\Omega$) in the rotating hub system if they are vertical shear or yaw moment, but at $kn\Omega \pm \Omega$ frequencies in the rotating hub system if they are in-plane shears, pitch or roll moments.

The parameters which affect the magnitude of fixed system $n\Omega$ loads include the number of blades, aerodynamic forces, blade response and fuselage response.

The aerodynamic forcing function which excites each blade can be represented as a Fourier series in Ωt since the time-history pattern repeats after each rotor revolution (for a given steady state flight condition). Measured results indicate that 1Ω and 2Ω airloads have the highest amplitudes; 3Ω, 4Ω, and 5Ω have approximately similar amplitudes but considerably less than 1Ω and 2Ω; 6Ω on up amplitudes are the smallest (see Figure 2.2). Combining this information with that of the previous paragraph leads to the conclusion that 2- and 3-bladed rotors, being exposed to the highest aerodynamic excitations of $n\Omega$ and $(n-1)\Omega$ will have the highest blade response and thus the highest $n\Omega$ fixed system rotor loads. Four and five-bladed rotors with substantially lower excitation at contributing frequencies should have lower $n\Omega$ fixed system rotor loads than 2- and 3-bladed rotors. Six and more bladed rotors should have the lowest $n\Omega$ fixed system rotor loads.

Blade response, and consequently blade root loads are very sensitive to the location of blade resonances relative to excitation frequencies. In an n-bladed rotor, the frequencies to avoid are $n\Omega$ and $n\Omega \pm \Omega$, and this becomes increasingly more difficult as the number of blades is reduced. Thus, the optimum blade resonance placement for achieving small $n\Omega$ fixed system loads is a function of the number of blades (e.g. a flap mode at 2.9Ω would be most detrimental on a 3-bladed rotor, but acceptable on a 2 or 5-bladed rotor). A preliminary design criterion consists of maintaining a 0.5Ω separation between contributing excitation frequencies and the closest blade resonances. This should yield reasonable blade response and consequently low blade root loads. Blade resonant frequencies and root loads are very strongly affected by the blade root end conditions, i.e. how the blade is attached to the hub. A teetering rotor is relatively free to pitch and roll about the hub center.

Therefore, it will transmit only linear forces plus yaw moment to the fuselage (no pitch or roll moments). An articulated rotor will transmit pitch, roll, and yaw moments to the fuselage in direct proportion to the flap and lag hinge offsets. A hingeless or rigid rotor transmits pitch as well as roll moments, and these excitation effects on the fuselage can be greater than those of linear forces.

The primary intent of minimizing main rotor loads is to reduce vibration levels in the fuselage. Consequently, the location of airframe resonances is extremely important since airframe response can be unacceptably high even with low rotor loads if a structural resonance should happen to be close to $n\Omega$.

In summary, the parameters most likely to render a total rotor isolation system highly desirable include

Low number of blades per rotor; 2 or 3 blades, then 3 or 4, 6 and more the least likely.

Blade resonance location close to $n\Omega$, or $n\Omega \pm \Omega$.

High fuselage response at $n\Omega$.

3. Total Main Rotor Isolation

During preliminary and final design stages of a new vehicle much effort is expended in optimizing the above parameters from a loads and vibration point of view. Nevertheless, when the prototype is flight tested, the vibration levels in the fuselage are sometimes excessive in spite of careful analytical and bench test efforts. At this stage, vibration control devices are tried and

if effective, become part of the production configuration. A total main rotor isolation system eliminates much of the trial-and-error testing of a helicopter configuration by ensuring very low nΩ fixed system main rotor loads.

3.1 The Rotor Isolation System

Total main rotor isolation, as defined in this study, is a long sought goal. The rotor imposes six vibratory loads at its n/rev forcing frequency. If these six loads are isolated, low helicopter vibration levels and the attendant benefits in crew performance, structural integrity and ride qualities will be realized.

In a matrix form, examine the vibration response at the cockpit in the vertical, lateral and longitudinal directions. The six components of rotor hub vibratory forces which produce three linear accelerations at the cockpit are illustrated in Figure 3.1-1. The forces applied to the fuselage after being modified by the transmission and its suspension are given by the "HUB TO FUSELAGE" transfer matrix. The accelerations produced at the cockpit as a result of the fuselage forces are given by the "FUSELAGE TO COCKPIT" transfer matrix. Thus, the cockpit accelerations are products of the two transfer matrices and the column of six hub forces and moments. The product of the "HUB TO FUSELAGE" matrix and the hub forces column give the fuselage forces at the lower right of Figure 3.1-1 and the product of the two transfer matrices gives the "HUB TO COCKPIT" transfer matrix (shown at the lower left in Figure 3.1-1), which yields the components of each of the three cockpit accelerations. When the transmission is rigidly attached to the fuselage all the matrix elements indicated are finite and, in general, complex valued.

In order to isolate the fuselage in every direction, all loads must be suppressed, and all the Sxy elements in the hub to fuselage transfer matrix, must be reduced to zero. The concept which Boeing will apply in order to achieve this goal is the Improved Rotor Isolation System, or IRIS. The IRIS is based on the passive antiresonant scheme first conceived by Kaman Aerospace Corp. and utilizes technology developed by Boeing Vertol for application to rotor isolation. The integral parts of an IRIS unit are a spring and an inertia bar, (see Figure 3.1-2). The spring connects the two bodies which are to be decoupled. One end of the inertia bar is attached to the transmission at pivot "X", and to the fuselage at pivot "F" a distance "r" from pivot "X" along the inertia bar. The CG of the bar is a distance "R" away from pivot "X". By proper choice of spring, bar geometry and mass combination, it is possible to generate an inertia force at the fuselage pivot "F" which is exactly equal and opposite to the spring force, thus preventing any net force, originating with the transmission, from acting on the fuselage at one frequency, ω_A, which is generally referred to as the antiresonant frequency. Deprived of excitation, the fuselage vibratory response is nulled (in the absence of damping) at $\omega=\omega_A$. The IRIS system consists of one bi-directional isolator unit installed between each of the four legs of the transmission and the airframe which is to be isolated, (see Figure 3.1-3. Each anti-resonant bar/spring combination isolates in the vertical and tangential directions (orientation reference is made with respect to the transmission) and is free to move radially with the transmission relative to the airframe. A radial spring is not needed for isolation but may be required in the mathematical model to represent inadvertent system stiffness in this direction. These four bi-directional IRIS units, functioning together as one system, isolate the fuselage from the transmission in 6 axes.

An analytical model was developed to evaluate this system and includes:

ITEM	DIRECTIONS FOR ISOLATION	INDEPENDENT FREEDOMS
Hub/Transmission	Vert, lat, long, pitch, roll, yaw	6
Fuselage	Vert, lat, long, pitch, roll, yaw	6
		DEPENDENT FREEDOMS
IRIS Unit(4)	Vert, inplane, axial	3 x 4 = 12
Cockpit Vibration	Vert, lat, long	3

Cockpit vibration and motion at the transmission feet above and below the isolation system are calculated under the action of six vibratory rotor hub loads. A mini-computer plot of cockpit vertical, lateral, and longitudinal vibration vs forcing frequency from 0 to 6/rev is provided. Vibration across the IRIS legs, i.e. transmission side forced vibration vs frequency from 90% of 4/rev to 110% of 4/rev, and the isolated airframe side, and the transmissibility are plotted. The resonant and antiresonant frequencies, steady and vibratory linear and angular deflections, spring deflections and loads are available from printed output.

3.2 The Baseline Aircraft

Three approaches to baseline aircraft applications are available to Boeing. First is the Company-owned BO-105, second is the CH-47, and third is a bailed Government-owned helicopter.

As the first alternative, the BO-105 is an existing flightworthy aircraft which has undergone one successful flight isolation program with a four-axis isolation system. The standard rotor-transmission installation of the BO-105 is shown in Figure 3.2-1. A tall transmission case is attached to the fuselage through a ring of bolts at the bottom and four truss-like struts. The struts carry lift and lateral/longitudinal loads at the top. A ring of bolts into the airframe at the bottom carry torque plus lateral/longitudinal loads. Moments are carried as differential couples at top and bottom, adding to lateral/longitudinal loads. In the current study installation, Figure 3.2-2, the transmission is supported more conventionally near its mid-level, but from the same airframe structure. A main rectangular frame will surround the transmission case at mid-level. The transmission case will be attached to the existing airframe hardpoints by a truss of strut members, thereby representing a more conventional transmission support arrangement. An inner ring is attached directly to the transmission case, with struts to the top of the case for stability. Interposed between the outer rectangular frame and the inner ring are the four bi-directional IRIS units. These will provide the six axis isolation, and will react all six rotor steady and vibratory loads. This arrangement will make the demonstration in the BO-105 more fully representative of an installation of a typical four-legged transmission case.

The second alternative is the CH-47D forward rotor which has a conventional four-legged transmission case. The possibility of isolation was considered in its design stage and space is provided for an eventual isolation system. The aft rotor of the CH-47D is more difficult to isolate. Its transmission is located on a lower deck, and thrust and radial bearings are provided at the

upper thrust deck location. A possible approach could be the development and demonstration of six axis rotor isolation on the forward rotor of this CH-47D aircraft. At a later time, isolation could be developed for the aft rotor.

A third alternative is a Government-owned aircraft for the program. A six axis isolation system could be developed for a helicopter other than the BO-105 or CH-47D above.

Of these three choices, the BO-105 is the most attractive and was selected as the baseline helicopter with government approval. Its main transmission/airframe interface is representative of many current helicopter installations (see Figure 3.2-3), and the aircraft is available for ground and flight test demonstration of the rotor isolation concept.

3.3 IRIS Performance Prediction

3.3.1 Rotor Isolation Design Criteria

Having selected the isolation system as well as the baseline helicopter, a set of design criteria was established to evaluate the system performance. This is summarized in Table 3.3-1.

As concluded in section 3.1, all main rotor loads have to be isolated, forces as well as moments. The isolation frequency of the BO-105 is 28.3 Hz (n/rev = 4/rev of 425 RPM). The isolation efficiency, defined here as $(1-Z_F/Z_X) \times 100$, Z_F/Z_X = fuselage-to-transmission motion ratio, is to be 95% within the frequency band of ±2%

of normal operating speed (425 RPM ± 8.5 RPM). Shaft misalignment is to be less than 1/2° steady ± 1/4° alternating to maintain troublefree shaft coupling operation. The isolation system shall attenuate main rotor loads in a maneuver environment of -.5G to + 1.5G. Outside of this range the system need not isolate, but motion transmissibility is not to exceed 1.0. The main rotor loads attenuated in the manner and to the degree specified above are taken as the baseline 1G level flight condition. The alternating portions are derived from a normal approach to landing which generates the highest vibratory main rotor loads on the BO-105.

Table 3.3-1 Isolation System Design Criteria

Isolation Directions	Longitudinal Lateral Vertical Roll Pitch Yaw	
Isolation Frequency	n/rev = 28.3 Hz	
Isolation Efficiency	95% of n/rev ± 2%	
Shaft Misalignment	1/2° ± 1/4°	
Maneuver Environment	-.5G + 1.5G	
Rotor Loads @ 1G		
Longitudinal	1780 ± 1780 N	400 ± 400 lb
Lateral	1780 ± 1780 N	400 ± 400 lb
Vertical	22560 ± 1780 N	5071 ± 400 lb
Roll	7840 ± 791 N-m	69400 ± 7000 in-lb
Pitch	7840 ± 1243 N-m	69400 ± 11000 in-lb
Yaw	10730 ± 1073 N-m	95000 ± 9500 in-lb

3.3.2 Tuning The System In 6 Axes

As indicated in section 3.1, the IRIS system consist of four isola-

tor units installed between each of the four transmission leg/airframe interface locations. The primary parts of each isolator (see Figure 3.3-1) are the inertia bar, spring, and pivots. The donut shaped tuning weight, W_T, combined with a bell shaped support, comprise the inertia bar. The spring is a cantilever beam, built in at the transmission end, but without angular restraint at the fuselage end. The last feature ensures that the spring load is transferred to the fuselage at a specific, accurately controlled, radius relative the transmission center, which is very important in maintaining concurrent tuning in the pitch and roll axes. The transmission pivot, P_x, having the same motion as the transmission, transfers this motion to the inertia bar. The fuselage pivot, P_F, a distance "r" from the transmission pivot, compels the inertia bar to move in compliance with the fuselage. The two pivots on the inertia bar couple the fuselage to the transmission by means of inertia loads in the vertical and tangential directions, while the spring performs a similar coupling function by means of spring loads. These inertia and spring loads can be readily adjusted to dynamically decouple the fuselage from the transmission in the vertical and tangential directions at one frequency, ω_A, by satisfying the relation

$$K - \omega_A^2 \, m \, [(R/r - 1) \, R/r + \rho^2/r^2] = 0 \qquad (3.3\text{-}1)$$

or $$K - \omega_A^2 \, M_{IA} = 0$$

where $$M_{IA} = m[(R/r - 1) \, R/r + (\rho/r)^2]$$

If equation 3.3-1 is satisfied simultaneously in three non-coplaner directions for each IRIS unit, the fuselage would be completely isolated from the transmission at the frequency $\omega = \omega_A$. However, a three directional IRIS unit would add more mechanical complexity to the system than is required. From a purely mathematical point of view only six independent degrees of freedom need to be isolated. Therefore, three bi-directional IRIS units arranged in a triangular pattern could perform the required task. However, from the point of view of redundant load paths for failsafety and applicability of the concept to existing transmission configurations, four bi-directional IRIS units represent a more reasonable choice.

The tuning requirements for an isolation system comprised of four bi-directional IRIS units, located with longitudinal and lateral symmetry around the azimuth, are derived in Appendix A and summarized in equations (3.3-2) through (3.3-5):

$$K_v = \omega_A^2 \, m \, [(R/r - 1) \, R/r + (\rho/r)^2] \qquad 3.3\text{-}2$$

$$K_\tau = K_v \qquad 3.3\text{-}3$$

$$K_r = 0 \qquad 3.3\text{-}4$$

$$\ell_s^2 = (\ell_x + r) \, \ell_x \qquad 3.3\text{-}5$$

Applying these tuning constraints to the reference configuration modeled in Figure 3.3-2, yields the following parameter values:

$$\omega_A = 2\pi \times 4 \times \frac{425}{60} = 178 \text{ rad/sec (n/rev = 4/rev)}$$

$$K_v = K_\tau = 4030000 \text{ N/m (23000 lb/in)}$$

$$K_r = 0$$

r = .0286 m (1.125) in (smallest value possible within constraints of bearing sizes)

R = -.159 m (-6.26) in (largest value possible within constraints of available space)

ρ = .0858 m (3.38) in (largest value possible within constraints of available space)

m = 2.808 kg (.016 lb-sec^2/in) (fallout after selecting K, ω_A, r, R, and ρ)

ℓ_x = .4858 m (19.125) in (determined by length requirement for main spring K_v, K_τ)

ℓ_s = $(\ell_x + r)\ \ell_x$ = .4999 m (19.68 in)

These parameters are now substituted into the minicomputer program described in section 3.1. An undamped forced sweep is calculated up to 6/rev, applying one rotor load at a time, and solving for all motions and loads of the transmission/IRIS/fuselage system (12 independent degrees of freedom). The rotor loads employed in this analysis, Table 3.3-1, are the highest encountered in the normal BO-105 1G level flight envelope.

3.3.3 Isolation Performance of Reference Configuration

Figure 3.3-3 shows the primary vibration response in dimensionless acceleration units of "G" at the pilot's station (see Figure 3.3-2) which is located 1.52 m (60 in.) forward of, .457 m (18 in.) to the right of, and .508 m (20 in.) below the aircraft CG, plotted against dimensionless frequency in units of per rev. The designation within the brackets below each response direction refers to the load which is applied at the rotor hub. The top left graph shows the vertical

cockpit response due to vertical hub load. The nonisolated (rigid body) response is .08G (zero frequency asymptote). The vertical resonance occurs at 3.11/rev, the antiresonance with zero response at 4.00/rev, as required. The next lower graph represents vertical cockpit response due to longitudinal hub load. Again, the antiresonance occurs at exactly 4/rev. The same is true for the vertical response due to pitch, lateral and roll.

The right hand column of Figure 3.3-3 presents the inplane response at the same cockpit location, lateral response due to yaw moment, longitudinal response due to longitudinal force, etc.. The antiresonant frequency is at exactly 4/rev in every case. The sharpest slopes of response near the 4/rev antiresonance occur with yaw excitation and will bear watching.

Dynamic response at a typical fuselage/transmission interface location is presented in Figure 3.3-4 for a narrow frequency band between .9 and 1.1 of 4/rev. Each row represents the response due to one rotor load. The leftmost column shows motion, in G units, on the fuselage (isolated) side of a typical IRIS unit, the middle column the motion of the transmission (driver) side of a typical IRIS unit, and the right column transmissibility, the ratio of fuselage-to-transmission motion. Vertical acceleration is indicated by the solid line, longitudinal by dots, and lateral by squares. Fuselage response in each of the three linear directions is nulled at 4/rev, no matter which rotor hub load is used to excite the system! Since each IRIS unit transmits only forces to the fuselage,

the collective effect of the four IRIS units is to isolate the fuselage in all 6 axes at 4/rev.

Lateral fuselage response to lateral hub excitation has the steepest slope near 4/rev, and therefore, the narrowest bandwidth of 4.2% within which the transmissibility is less than or equal to .05 (95% isolation). All other responses show wider bandwidths, thus satisfying the isolation efficiency criterion (see Table 3.3-1).

Steady deflections and loads, applicable to design of spring stroke and load carrying requirements, are presented in Table 3.3-2. Numbers in the two top rows represent the forces (first row) and moments (second row) which are applied at the rotor hub. The next six rows show the longitudinal, lateral, and vertical displacements of the transmission CG relative to the fuselage due to each individual rotor hub load. The rightmost column shows the maximum possible value for each deflection if the most unfavourable phasing between the hub loads is assumed (such that their effects add). Thus the maximum possible longitudinal, lateral and vertical transmission CG deflections are .117, .117, and .136 cm, respectively (.0461, .0461, and .0537 inches). The next group of numbers, representing steady transmission angles relative to the fuselage, indicate maximum values of .268, .268, and .153 degrees in roll, pitch and yaw, respectively, whose vector sum yields .41 degrees, well below the .5 degree limit criterion (see Table 3.3-1). Maximum deflections in the tangential, radial, and vertical springs are .164, .031, and .467 cm (.0647, .0122, and .1837 inches) (radial spring has zero rate in this refer

TABLE 3.3-2 STEADY DEFLECTIONS AND LOADS
REFERENCE CONFIGURATION, 6 AXIS IRIS

		LONGITUDINAL ROLL	LATERAL PITCH	VERTICAL TORQUE	MAXIMUM SUM
FORCES	N (LB)	1779 (400)	1779 (400)	21980 (4941)	
MOMENTS	N-M (LB-IN)	7341 (69400)	7841 (69400)	10730 (95000)	
XMSN CG CM (IN)	LONG	.0378 (.0149)	.0 (.0)	.0 (.0)	
		.0 (.0)	-.0792 (-.0312)	.0 (.0)	.1171 (.0461)
	LAT	.0 (.0)	.0378 (.0149)	.0 (.0)	
		.0792 (.0312)	.0 (.0)	.0 (.0)	.1171 (.0461)
	VERT	.0 (.0)	.0 (.0)	.1389 (.0537)	
		.0 (.0)	.0 (.0)	. (.0)	.1389 (.0537)
XMSN ANGLE DEG	ROLL	.0	.045	.0	
		.223	.0	.0	.268
	PITCH	-.045	.0	.0	
		.0	.223	.0	.268
	YAW	.0	.0	.0	
		.0	.0	.153	.153
SPRING DEFL CM (IN)	TANGENTIAL	.0155 (.0061)	.0155 (.0061)	.0 (.0)	
		.0 (.0)	.0 (.0)	.1334 (.0525)	.1644 (.0647)
	RADIAL	.0155 (.0061)	.0155 (-.0061)	.0 (.0)	
		.0 (.0)	.0 (.0)	.0 (.0)	.0310 (.0122)
	VERTICAL	.0274 (.0108)	.0274 (-.0108)	.1364 (.0537)	
		.1377 (-.0542)	.1377 (-.0542)	.0 (.0)	.4666 (.1837)
SPRING LOAD N (LB)	TANGENTIAL	627 (141)	627 (141)	0 (0)	
		0 (0)	0 (0)	5369 (1207)	6623 (1489)
	RADIAL	0 (0)	0 (0)	0 (0)	
		0 (0)	0 (0)	0 (0)	0 (0)
	VERTICAL	1108 (249)	1108 (-249)	5439 (1235)	
		-5547 (-1247)	-5547 (-1247)	0 (0)	18802 (4227)

TABLE 3.3.-3 4/REV MOTIONS AND LOADS
REFERENCE CONFIGURATION, 6 AXIS IRIS

		LONGITUDINAL ROLL	LATERAL PITCH	VERTICAL TORQUE	MAXIMUM SUM
FORCES N (LB)		1779 (400)	1779 (400)	1779 (400)	
MOMENTS N-M (LB-IN)		847 (7500)	1243 (11000)	1073 (9500)	
XMSN CG ACC G	LONG	-.5278	.0	.0	
		.0	.0347	.0	.5625
	LAT	.0	-.5278	.0	
		-.0236	.0	.0	.5514
	VERT	.0	.0	-.4482	
		.0	.0	.0	.4482
XMSN ANGLE DEG	ROLL	.0	-.0304	.0	
		-.0207	.0	.0	.0511
	PITCH	.0304	.0	.0	
		.0	-.0304	.0	.0608
	YAW	.0	.0	.0	
		.0	.0	-.0616	.0616
SPRING DEFL CM (IN)	TANGENTIAL	-.0041 (-.0016)	-.0041 (-.0016)	.0 (.0)	
		.0046 (.0018)	-.0069 (-.0027)	.0538 (-.0212)	.0734 (.0289)
	RADIAL	-.0041 (-.0016)	.0041 (.0016)	.0 (.0)	
		-.0046 (-.0018)	-.0069 (-.0027)	.0 (.0)	.0196 (.0077)
	VERTICAL	-.0188 (-.0074)	.0188 (.0074)	.0140 (-.0055)	
		.0127 (.0050)	.0188 (.0074)	.0 (.0)	.0831 (.0327)
SPRING LOAD N (LB)	TANGENTIAL	-160 (-36)	-160 (-36)	0 (0)	
		187 (42)	-276 (-62)	-2166 (-487)	2949 (663)
	RADIAL	0 (0)	0 (0)	0 (0)	
		0 (0)	0 (0)	0 (0)	0 (0)
	VERTICAL	-756 (-170)	756 (170)	-560 (-126)	
		516 (116)	756 (170)	0 (0)	3345 (752)

ence configuration). Maximum tangential and vertical spring loads are 6623 and 18000 N (1489 and 4227 lb), respectively.

Alternating motions and loads at 4/rev are presented in Table 3.3-3 in the same format as the steady results. Maximum longitudinal, lateral and transmission accelerations at 4/rev are .5025, .5514, and .4482 G, respectively. Maximum angular excursions of the transmission are below .07 degrees, spring deflections below less than 0.1 cm (.04 in). Maximum alternating spring loads are 1361 N (603 lb) tangentially and 3344 N (752 lb) vertically.

3.4 Variation of System Parameters

The reference configuration described in section 3.3.3 satisfied or exceeded all the design criteria of Table 3.3-1. Sensitivity in the performance of this isolation system to perturbations of its parametric values are evaluated in this section.

3.4.1 Mount Plane Variation

Changing the waterline at which the in-plane loads are transferred through the IRIS units to the fuselage alters the kinematic relationship between the system inertia and its spring constraints, so that one of the first consequences of such a variation should be a shift in system resonances. This is demonstrated in Figure 3.3-5 in which the waterline of hub, transmission CG, and airframe CG were kept constant while moving the waterline of the in-plane transmission/fuse-

lage interface. The reference configuration with a .204 m (8 inch) separation between the transmission CG and the mount plane below, has the longitudinal mode at the lowest frequency (2.56/rev) followed by the lateral mode (2.73/rev), then pitch (2.97/rev) roll (2.99/rev), vertical (3.11/rev) and yaw (3.59/rev). As the mount plane is lowered, the lateral and longitudinal resonances drop in frequency, those of pitch and roll increase, while the vertical and yaw resonances are unaffected.

As a resonance approaches the antiresonant frequency which is maintained at 4/rev, the isolation system must work harder and harder to decrease the high fuselage response at that resonance to a null at the antiresonant frequency. This leads to increasingly steeper slopes of airframe response versus frequency near 4/rev, and decreasingly smaller frequency bands over which a constant value of transmissibility, e.g., .05, is maintained. The opposite effect is obtained if a resonance is moved further away from the antiresonance. Figure 3.3-6 illustrates this effect by comparing the transmissibilities of the reference configuration with a mount plane .203 m (8 inches) below the transmission CG to one with .508 m (20 inches) below. From Figure 3.3-5 it can be predicted that the .508 m (20 inch) configuration, having lower frequency longitudinal and lateral modes, would have shallower response slopes for longitudinal and lateral hub loads than the .203 m (8 inch) reference configuration, and that the opposite trend would occur for the response to pitch and roll hub moments. Vertical and yaw response is unaffected since the modes in these two axes are not changed by mount plane variations.

Mount plane height variation provides a means of trading off low transmissibility bandwidths in the longitudinal and lateral directions against those in the pitch and roll directions, without influencing vertical and yaw.

3.4.2 Spring Rate Variation

A change in spring rate will not only alter the steady deflections in inverse proportion but will shift resonances as well. Table 3.4-1 summarizes an arbitrary ±525000 N/m (±3000 lb/in) variation in vertical spring rate. The resonance changes by only ±2%, due to the fact that since the system is kept tuned to a constant antiresonance of 28.3 Hz (4/rev), the inertia bar weight changes in direct proportion (±13%) with the spring rate, while the system mass is not changed in the same proportion.

Table 3.4-1 Spring Rate Effect On Resonance and Bar Weight

SPRING RATE N/m (lb/in)	RESONANCE PER REV	INERTIA BAR WT kg (lb)
$3.5X10^6$ (20000) (-13%)	3.04 (-2%)	2.44 (5.38) (-13%)
$4.03X10^6$ (23000)	3.11	2.81 (6.19)
$4.55X10^6$ (26000) (+13%)	3.18 (+2%)	3.18 (7.00) (+13%)

Figure 3.3-7 shows the effects of such an IRIS spring rate change on transmissibility. The vertical and tangential spring rates were varied simultaneously while maintaining constant 4/rev antiresonant tuning by adjusting the inertia bar weights as required. Softer springs (left most column) yield lower resonances, thus shallower

slopes near 4/rev, whereas stiffer springs (right most column) yield the opposite results.

The reference configuration is in the middle column. Lateral response has the narrowest bandwidth for which transmissibility is less than .05 (95% isolation), and this bandwidth, 4.2% N_R for the reference configuration, increases to 5.5% of N_R with the softer spring, and decreases to 3.5% of N_R with the stiffer 4.55×10^6 N/m (26000 lb/in) spring.

A 13% change in spring rate yields only a 1.3% change in bandwidth. The IRIS system's isolation performance is relatively insensitive to spring rate variations which might occur in actual hardware.

The nominal IRIS spring rate of 4.03×10^6 N/m (23000 lb/in) in the vertical and tangential directions, as well as the softening excursion, meet the 95% isolation bandwidth criterion in all axes; the stiffer spring rate does not.

Thus, the 4.03×10^6 N/m (23000 lb/in) spring rate for each IRIS unit, or 16.11×10^6 N/m (92000 lb/in) per aircraft, represents an upper bound. Even though higher values might seem desirable from the point of view of small transmission deflections, low shaft misalignment angles, and easier flight control discoupling task, this spring rate is already very stiff. If a conventional passive isolation system were to provide 95% isolation (.05 motion transmissibility) between the 331 kg (730 lb) transmission and 1910 kg (4211 lb) fuselage at

28.3 Hz, the system resonance would have to be at 6.176 Hz and the total spring rate 424858 N/m (2426 lb/in). The resulting steady state vertical displacement between the fuselage would be .043 m (1.7 inches), a prohibitively high value compared to the .0013 m (.05 inch) deflection for the reference configuration above.

Although a softer spring rate yields lighter inertia bar weights, it increases deflections and shaft misalignments, and lowers the resonant frequencies which might adversely affect handling qualities.

3.4.3 Inertia Bar Weight/Geometry Variation

The sign convention used in this report utilizes the transmission pivot as the measurement reference point for pivot separation and bar CG. When the vector drawn from the transmission pivot towards the fuselage pivot points in the same direction as the vector from the transmission pivot to the bar CG, the ratio R/r is called positive. If these two vectors point in opposite directions, the ratio R/r is called negative.

In this context, the tuning equation (3.3-1) has two solution branches, one having positive, the other negative values of R/r. It is obvious that if R/r = 6 satisfies equation (3.3-1), so does R/r = -5, or if R/r = 7 is a solution, so is -6, etc, assuming that all other parameters remain constant. Each pair of these solutions, like R/r = 6 and -5, represent one and the same physical inertia bar, but turned end for end and reconnected to the transmission and

fuselage. The configuration shown in the schematic of Figure 3.3-8 represents a positive R/r. Bar orientation does not affect tuning, but it does alter resonances, negative R/r yielding slightly lower frequencies than positive R/r values.

The trade-off between inertia bar weight and geometry is fairly straight forward: the larger the ratio of bar CG to pivot separation, the smaller the required bar weight, as shown in Figure 3.3-8. The two R/r scales represent the two possible solutions. Large R/r values are limited by the geometric and configuration constraints. For a positive R/r, the inertia bar, starting at end of the IRIS spring, points radially outward away from the transmission center, and beyond the aircraft contour. A negative R/r turns the inertia bar around and points it from the end of the spring radially inward towards the transmission center, permitting a more compact installation.

The negative R/r configuration was chosen for the BO-105 in an effort to keep the IRIS system installation within the confines of the existing aircraft contours. But available space is limited and while locating the transmission pivot as far outboard as possible (aircraft contour limit), and the tuning weight as far inboard as possible (limit is transmission case structure), the maximum magnitude of R/r attainable with the reference configuration is 5.56 (negative), requiring a bar weight of 2.81 kg (6.2 lb) for each of the four units.

3.4.4 Radial Spring Rate

A radial spring is not required for proper operation of the IRIS system, as described in section 3.1, but the fuselage fitting of each IRIS unit (see Figure 3.3-1) incorporates an elastomeric bearing which is very stiff in the vertical and tangential directions and as soft as possible in the radial direction. A finite value in the radial spring rate will detune the system and the sensitivity of this radial spring on isolation performance is discussed below. A value less than 5% of the main spring appears to be attainable. Figure 3.3-9 shows the cockpit response with 175000 N/m (1000 lb/in) radial spring rate (4.3% of main spring rate) added to the reference configuration. Half of the responses remain nulled at 4/rev and the response levels of the other degrees of freedom are very low. A clearer understanding of this effect may be gained by looking at the transmissibilities at a typical transmission/fuselage interface, Figure 3.3-10. Longitudinal and lateral response nulls occur at a frequency slightly above 4/rev (about 1%). Vertical and yaw are unaffected. Roll and pitch do not have a null response frequency, but their transmissibility values, as well as those of longitudinal and lateral axes, are on the order of 0.02 at 4/rev. The relatively narrow bandwidths of the lateral and longitudinal transmissibility can be traded off against the currently wide bandwidths in pitch and roll by increasing the separation between the transmission CG and the mount plane below, as discussed in Section 3.3.3. This would compensate the detuning effect of a finite radial spring rate in the longitudinal and lateral axes, by widening their bandwidths, thus

achieving the same degree of isolation over the same frequency range around 4/rev as the reference configuration.

3.4.5 System Damping

The magnitude of system damping was estimated by assuming that the contribution from the main spring and its associated load paths was equivalent to a structural damping constant of g = .02 (this corresponds to a modal damping of .01 or 1% critical). The primary spring alone has very little damping; an individual IRIS unit has in the past exhibited structural damping on the order of g = .01, but when installed in an aircraft as a complete system, the resulting system damping has been on the order of g = .02 in flight test of the BO-105 4-axis IRIS. Elastomeric bearings which serve as pivots in each IRIS unit were assumed to have much larger damping of g = .09.

Referring to Figure 3.3-1, the spring rates of bearings to be used in a BO-105 IRIS unit are

transmission pivot bearing	571 N-m/rad (4580 in lb/rad)
fuselage pivot bearing	517 N-m/rad (4580 in lb/rad)
spring pivot bearing	491 N-m/rad (4350 in lb/rad)
radial spring of fuselage fitting	175000 N/m (1000 lb/in)

If the deflection of the transmission relative to the fuselage is δ meters, then the fuselage and transmission bearings rotate through the same angle of δ/r, where r is the pivot separation. The spring pivot bearing undergoes a smaller rotation, conservatively estimated

to be the same as the end rotation of an unrestrained main spring, namely $\theta = .29\delta$ for this configuration. The radial spring is conservatively assumed to undergo the same deflection as the transmission, δ.

Summing up all these damping contributions, keeping in mind that the energy taken out of the system during one complete cycle of motion is given by

$$E = \Sigma \pi K_i g_i \delta_i^2 \quad \ldots\ldots\ldots\ldots\ldots (3.4.5\text{-}1)$$

which leads to

$$E = \pi [K_v g_v \delta^2 + 2K_p g_p \left(\frac{\delta}{r}\right)^2 + K_s g_p (.29\delta)^2 + K_r g_p \delta^2]$$

$$= \pi K_v \delta^2 [g_v + \frac{2K_p}{K_v r^2} g_p + \frac{K_s}{K_v} (.29)^2 g_p + \frac{K_r}{K_v} g_p]$$

$$= \pi K_v \delta^2 [g_v + .315\, g_p + .016\, g_p + .043\, g_p]$$

$$= \pi K_v \delta^2 [.02 + .374\ (.09)] = \pi K_v \delta^2\ (.054). \quad \ldots\ldots (3.4.5\text{-}2)$$

In terms of fraction of total system damping of $g_{syst} = .054$, the main spring contributes 37% and the two pivot bearings 52.5%, the remaining 10.5% being shared by the main spring bearing and the radial spring in the fuselage fitting.

An estimate of isolation degradation of the system due to damping can be quantified by realizing that the only forces acting on the isolated fuselage at the antiresonant frequency result from damping, i.e. $Kg\delta$, where δ is the relative motion between transmission and fuselage. The sum of all other loads, which are 90° out of phase

with the damping force, is zero. The remaining forces are reducable to combinations of terms involving

$$K - \omega_A^2 M_{IA} \qquad (3.4.5\text{-}3)$$

which are zero by definition.

At the antiresonant frequency the fuselage is subjected only to damping loads of the type $Kg\delta$, and the degree of isolation (for a simple unidirectional system) is given by

$$I_{\omega=\omega_A} = 1 - \frac{Z_F^{\text{Isolated}}}{Z_F^{\text{Nonisolated}}}$$

$$= 1 - \frac{g}{\sqrt{(1 - \omega_A^2/\omega_R^2)^2 + g^2}} \qquad (3.4.5\text{-}4)$$

where

ω_A = antiresonant frequency

ω_R = coupled system resonant frequency

Isolation is plotted against the frequency ratio ω_A/ω_R in Figure 3.3-11. Since ω_A is constant at 4/rev (28.3Hz), an increase in ω_R would cause us to move from right to left along any one of the constant damping (g) curves. The reference configuration with 5% structural damping would achieve 92% isolation at a frequency ratio of 1.29, as indicated.

3.5 System Weight

The weight estimate of the baseline configuration is given in the left hand column of Table 3.5-1 and includes all weights which would have to be removed to convert the isolation system into a rigid transmission/fuselage interface. This includes inertia bars, bearings and springs. (The fuselage fitting bearings was considered to part of the airframe, as well as the rectangular frame around the transmission). As listed, the system weighs 29.53 kg (65.1 lb), which is 1.28% of the 2300 kg (5071 lb) DGW, or 9.53 kg (14.4 lb) over the design goal of 23 kg (50.7 lb) (1% of DGW). The system weight can be optimized to the goal of 23 kg (50.7 lb) during the detail design phase by

Substituting composite material for aluminum in the tuning weight support, thus increasing the bar CG separation from the transmission pivot which results in a smaller tuning weight requirement.

Substituting composite material for steel in the springs and accounting for structural weight which would have to be included for a rigid installation, i.e. transmission feet; no such weight credit was taken in the estimate above.

Careful selection of bearing options with special attention to weight reduction.

The projected detail design weights are shown in the right-hand column of Table 3.5-1 at 22.86 kg (50.4 lb), slightly under the 23.0 kg (50.7 lb) (1% DGW) design goal.

Table 3.5-1 System Weight Estimate

	Reference Configuration kg (lb)	Projected Detail Design kg (lb)
Inertia Bars (4)	11.25 (24.8)	9.25 (20.4)
Bearings (12)	11.16 (24.6)	10.44 (23.0)
Springs (4)	7.12 (15.7)	4.76 (10.5)
Credit for rigid installation (33% of spring weight)	0 (0)	-1.59 (-3.5)
System Weight	29.53 (65.1)	22.86 (50.4)
1% A/C DGW	23.00 (50.7)	23.00 (50.7)
Delta Weight (from 1% A/C DGW)	+6.53 (+14.4)	-.14 (-.3)

3.6 Dual Frequency Capability

An IRIS system can be designed to provide two simultaneous anti-resonances, should this requirement arise. By adding a spring mass to the inertia bar, Figure 3.6-1, the IRIS unit becomes capable of multi-frequency isolation. This concept has been successfully flight-tested on the BO-105, Reference 2.

3.7 Risk Evaluation

Real hardware and system performance deviate from their design goal values to a smaller or greater extent, depending on the validity of the mathematical model used in the analysis, the depth of understanding and anticipating important system interactions, and control of manufacturing tolerances. The certainty with which each major system parameter and performance goal will be attained is estimated and summarized in Table 3.7.1.

The vertical and tangential spring rate values are accurately attainable within the uncertainty of the back-up structure spring rate, which will tend to lower the resultant stiffness, thus lowerng the anti-resonant frequency. Proper tuning is easily maintained by adjusting the tuning weights. The certainty of achieving the 4.03×10^6 N/m (23000 lb/in) system spring rate (per IRIS unit) is estimated at 95%.

The radial spring rate of each IRIS unit is not as easily controlled as the vertical and tangential above, for it is a fallout of the fuselage fitting bearing which should be as stiff as possible in the other two directions. The 1.75×10^5 N/m (1000 lb/in) rate detunes the system by 1%, which cuts into the isolation bandwidth. This effect can be compensated by lowering the mount plane relative to the transmission CG to broaden the isolation bandwidth. The certainty of keeping the radial spring rate below 1.75×10^5 N/m (1000 lb/in) (per IRIS unit) is estimated at 70%.

TABLE 3.7-1 RISK EVALUATION SUMMARY

DESIGN PARAMETER	DESIGN VALUE	ESTIMATED CERTAINTY OF ACHIEVING DESIGN VALUE (%)	EFFECT OF UNDERACHIEVING DESIGN VALUE	POTENTIAL REMEDY
Vertical spring rate	4030000 N/m (23000 lb/in)	95	Detuning	• Adjust tuning weight
Tangential spring rate		95	Detuning	• Adjust tuning weight
Radial spring rate	175000 N/m (1000 lb/in)	70	Detuning	• Lower mount plane to widen isolation bucket
System damping	$g \leq .054$	80	Reduced isolation efficiency	• Change elastomer material in bearings • Soften spring rates
Isolation efficiency	95% @ 4/rev$\pm$2%	90	Increased fuselage vibration at 4/rev	• Decrease system damping • Soften spring rates • Lower mount plane
Shaft misalignment	$.5^{o} \pm .25^{o}$	95	Reduced coupling	• Introduce steady offset • Bring mount plane closer to Xmsn CG • Stiffen spring rates
System Weight	1% of DGW	80	Overweight	• Increase R/r • Lower spring rates

High system damping leads to reduced isolation efficiency and higher fuselage vibration. In the selection of elastomeric materials which will be used in the bearings, special attention will be paid to attaining low damping characteristics as well as to reducing the angular spring rates to minimum possible values. If the spring rate is low enough, the impact on system damping can be small even if the material itself has high structural damping. The certainty of keeping the system damping below g = .054 is estimated at 80%.

Isolation efficiency shortcomings will be reflected in elevated fuselage vibration levels at 4/rev. This can be alleviated by decreasing damping, reducing the spring rates, lowering the mount plane relative to the transmission cg, or a combination of these. The certainty of achieving 95% isolation at 4/rev ± 2% is estimated at 90%.

Excessive shaft misalignment, which reduces shaft coupling life expectancy, can be controlled by introducing a steady offset angle during installation (transmission relative to fuselage), bringing the mount plane closer to the transmission CG, or increasing the spring rates. The certainty of keeping the misalignment angles below .5° ± .25° is estimated at 95%.

The reference configuration isolation system weighs 29.53 kg (65.1 lbs), 6.53 kg (14.4 lb) over the 1% DGW target of 23.0 kg (50.7 lb). The certainty of achieving the target weight by utilizing composites in the tuning weight support and springs is estimated at 80%.

3.8 Handling Qualities and Stability

Based on the favorable flight experience with the 4-axis IRIS on the BO-105, no adverse effects are anticipated in expanding the same type isolation system to 6 axis. The BO-105 design was characterized by the absence of degradation in handling qualities and stability margins relative to the untreated aircraft configuration within the normal flight envelope. The flight controls will be decoupled so that transmission motion will not induce false command signals in the actuators.

3.9 Reliability and Maintainability

Helicopter operators appreciate that helicopters with low vibration levels are not only popular with the passengers and flight crew because of the increased comfort, but the reduced vibration favorably impacts the helicopter reliability (R) and maintainability (M); the helicopter subsystems experience fewer failures. Reference (6) reports on a controlled flight program with and without a hub mounted vibration absorber and quantifies a substantial R and M saving associated with the reduced vibration level of the vibration absorber equipped helicopter.

The R & M gains achieved by vibration reduction appear to far out-weigh any additional complexity which accompanies a rotor isolation system. An assessment of the impact of the main rotor isolation system on the overall helicopter R and M is beyond the scope of this study. However, this study will access the maintenance action rate in terms of mean time between failure (MTFB) hours, where "failure" is defined as an unscheduled maintenance action, and maintenance manhours per flight hour (MMF/FH) resulting from components peculiar to the main rotor isolation system installation in a BO-105 helicopter. The components assessed include those of the isolator and those additional components in the flight controls and drive system necessary to apply the isolation system.

The main rotor isolation system is shown schematically in Figure 3.2-2. The system shown consists of the four isolators which isolate the rotor transmission system from the airframe, and some new structural components

which are necessary to install the isolators in the BO-105 using the present transmission housing with minimum modification to the airframe structure. These structural components are the inner ring between the isolators and the airframe. As the ring and frame would not be included in an aircraft designed for the rotor isolation system in the basic concept and there would be no equivalent components necessary, these components are excluded from the R & M analysis.

Tables 3.3-2 and 3.3-3 give the steady and alternating motions between the airframe and rotor-drive system resulting from incorporation of a rotor isolation system. These motions impact the design of the flight controls and drive systems as follows:

Flight controls system

Two bellcranks and connecting linkages are necessary in each of the three main rotor flight control axes (collective, lateral and longitudinal) to prevent motion feedback into the controls.

A fly-by-wire system with the actuators mounted on the transmission housing would be free of any control input motion feedback without the use of the above bellcranks.

Drive System

An additional flexible coupling or additional stages to an existing Bendix type flexible coupling is necessary in the two

engine shafts, and the tail rotor drive shaft to accommodate the increased flexing which will occur in these shafts. Additional stages were added to the production BO-105 prior to the flight test evaluation of the 4-Axis IRIS. The modified couplings performed successfully throughout the program which lasted 180 flights.

Table 3.9-1 gives an assessment of the reliability and maintainability characteristics of the main rotor isolator, the modifications to the flight controls system and the modifications to the drive system. The values for MTBF (mean time between failure-malfunction) are based on experience with similar components in current helicopters. The maintenance manhours to remove and replace components are assessments based on the complexity of the task assuming these components had been installed in a helicopter which considered the isolation system in the initial structural design.

This assessment predicts an overall maintenance action rate for the main rotor isolation system and associated flight control and drive system components of .00571 malfunction per flight hour (175 hours MTBF). The system maintenance manhours per flight hour is .0083.

Overall aircraft maintenance action rates and maintenance manhour rates are not available for the BO-105 helicopter; however equivalent values are given in U.S. Army data for the OH-58A helicopter and are probably "order of magnitude" values for a small helicopter. These values of 1.7 malfunctions per flight hour and 2.0 maintenance manhours per flight hour

TABLE 3.9-1

ASSESSMENT OF RELIABILITY AND MAINTAINABILITY CHARACTERISTICS

COMPONENT	QTY	DESCRIPTION	MTFB[1], HOURS COMPONENT	F/MFH[2] ASSY	M/H TO REM/REP[3] COMPONENT	MMH/MFH[4]
1. ISOLATOR (FIG. 2.3-1)	(4)		-	-	1.4	1028
1.1 FUSELAGE FITTING	(1)	METAL SLEEVE	1,000,000	1	.3	.3
1.2 RADIAL SPRING (FUSELAGE FITTING)	(2)	ELASTOMERIC BRG	20,000	100	.5	50
1.3 FUSELAGE PIVOT	(1)	METAL SHAFT, NUT	1,000,000	1	1.0	1.0
1.4 FUSELAGE PIVOT BASE	(1)	ELASTOMERIC BRG	5,000	200	1.0	200
1.5 XMSN PIVOT BRG	(1)	ELASTOMERIC BRG	5,000	200	1.0	200
1.6 TUNING WT SUPP.	(1)	METAL TUBE	1,000,000	1	.8	.8
1.7 TUNING WT	(1)	METAL	1,000,000	1	.2	.2
1.8 XMSN PIVOT SHAFT	(1)	METAL TUBE	1,000,000	1	1.0	1.0
1.9 XMSN SHAFT FITTING	(1)	FORGING	100,000	10	.5	5.
1.10 IRIS SPRING ASSY	(1)	FORGING	50,000	20	1.0	20
1.11 SPRING, PIVOT	(1)	ELASTOMERIC BRG	5,000	200	1.0	200
		UNIT ISOLATOR	1362	734	-	1706
		A/C ISOLATOR (4)	340	2936	-	6824
2. CONTROL MODIFICATIONS						
BELLCRANKS	(6)	ALUM. FORGING	100,000	60	.5	30
LINKAGES	(3)	SWAGED TUBING	50,000	60	.3	18
BEARINGS(IN LINKAGES)	(12)	TEFLON FABRIC	5,000	2,400	.5	1200
SUPPORTS	(2)	ALUM. FORGING	100,000	20	.5	10
HARDWARE	(20)	BOLTS, NUTS, WASHERS	100,000	200	.2	40
TOTAL CONTROLS			365	2740		1298
3. FLEXIBLE COUPLING	(3)	BENDIX TYPE (BASED ON CH-47 THOMAS COUPLING)	80,000	36	5	180
TOTAL COUPLING			27777	36		180
TOTAL ALL SYSTEMS			175	5712		8302 MMH PER MILLION FLIGHT HOURS

(1) MEAN TIME BETWEEN FAILURE (UNSCHEDULED MAINTENANCE ACTION), HOURS
(2) FAILURES PER MILLION FLIGHT HOURS
(3) MANHOURS TO REMOVE AND REPLACE COMPONENT OR ASSEMBLY
(4) MAINTENANCE MANHOURS PER MILLION FLIGHT HOURS

show that the adverse R and M impact of a rotor isolation system is negligible in terms of the overall helicopter R & M characteristics and the potential exists for a significant improvement in R & M characteristics of helicopter subsystems due to the reduced vibration levels which result from the incorporation of a rotor isolation system.

4. Recommendations for Ground and Flight Test Demonstration Program

The steps leading up to a successful flight demonstration of the IRIS isolation system are listed in the time-phased Figure 4-1. Isolation system loads and stress analysis as well as aeromechanical stability analysis will be finalized concurrently with detail design of aircraft modifications and IRIS system. Procurement of parts and manufacture of hardware precedes installation of the IRIS system into the modification aircraft, followed by an aircraft ground shake test, culminating in ground and flight test evaluation 24 months after go-ahead.

Of the six IRIS units, four are to be installed in the test aircraft, one is to be used in bench test evaluation, one is to be kept as a spare unit. The bench test of a single unit will empirically confirm the predicted dynamic spring rates, tuning capabilities, isolation performance and damping values. This information is used to reduce exploratory shake testing of the more complex total aircraft configuration. The same isolator unit will be subjected to a fatigue and proof load test.

The aircraft ground shake test will confirm the predicted system tuning and isolation efficiency for each individually applied hub load. This is impossible to accomplish in flight because all the loads are applied simultaneously and other non-isolated excitations are present such as aerodynamic blade downwash at n/rev. Aircraft static loads tests will be accomplished after the ground shake test.

Following the safety of flight review, the aircraft will undergo mechanical instability and hover checks, followed by handling quality checks in forward flight and acquisition of isolation system performance data. The first flights may necessitate minor tuning adjustments in order to utilize the isolation system's potential more efficiently.

References

1. Flannelly, W. G.: The Dynamic Antiresonant Vibration Isolator. Paper presented at the 22nd Annual National Forum of the American Helicopter Society, Washington, D. C., May 1966.

2. Desjardins, R. A.; and Hooper, W. E.: Rotor Isolation of the Hingeless Rotor BO-105 and YUH-61A Helicopters. Paper No. 13, presented at the 2nd European Rotorcraft and Powered Lift Aircraft Forum, September 1976.

3. Hooper, W. E.; and Desjardins, R. A.: Antiresonant Isolation for Hingeless Rotor Helicopters. Paper No. 760893, presented at SAE Aerospace Meeting, San Diego, California, December 1976.

4. Desjardins, R. A.; and Hooper, W. E.: Antiresonant Rotor Isolation for Vibration Reduction. Paper No. 78-24, presented at the 34th Annual National Forum of the American Helicopter Society, Washington, D. C., May 1978.

5. Desjardins, R. A.; and Sankewitsch, V.: Integrated Fuel/Floor Isolation System for Model 234 Commercial Chinook. Paper No. 39, presented at Fifth European Rotorcraft and Power Lift Aircraft Forum, September 1979, Amsterdan, Netherlands.

6. Veca, A.C.; Vibration Effects on Helicopter Reliability and Maintainability. USAAVLABS TR73-11, Eustis Directorate, U.S. Army Air Mobility Research and Development Laboratory, Fort Eustis, Virginia, 1973.

APPENDIX A

Tuning Equations for 6-Axis IRIS System

The tuning requirements for the 6-axis IRIS system are derived from equation (B-1) (Appendix B) by setting all components of fuselage motion equal to zero. The conditions which must be satisfied become:

Longitudinal

$$(K_\tau - \omega_A{}^2 M_{IA})\cos^2\theta + K_r \sin^2\theta = 0 \quad \ldots\ldots\ldots\ldots \text{(A-1)}$$

Lateral

$$(K_\tau - \omega_A{}^2 M_{IA})\sin^2\theta + K_r \cos^2\theta = 0 \quad \ldots\ldots\ldots\ldots \text{(A-2)}$$

Vertical

$$K_v - \omega_A{}^2 M_{IA} = 0 \quad \ldots\ldots\ldots\ldots\ldots\ldots\ldots\ldots \text{(A-3)}$$

Roll

$$\left.\begin{aligned} (K_\tau - \omega_A{}^2 M_{IA})\sin^2\theta + K_r \cos^2\theta &= 0 \\ \left[K_v \frac{\ell_s{}^2}{(\ell_x + r)\ell_x} - \omega_A{}^2 M_{IA}\right]\cos^2\theta &= 0 \end{aligned}\right\} \quad \ldots\ldots\ldots\ldots \text{(A-4)}$$

Pitch

$$\left.\begin{aligned} (K_\tau - \omega_A{}^2 M_{IA})\cos^2\theta + K_r \sin^2\theta &= 0 \\ \left[K_v \frac{\ell_s{}^2}{(\ell_x + r)\ell_x} - \omega_A{}^2 M_{IA}\right]\sin^2\theta &= 0 \end{aligned}\right\} \quad \ldots\ldots\ldots\ldots \text{(A-5)}$$

Yaw

$$K \frac{\ell_s{}^2}{(\ell_x + r)\ell_x} - \omega_A{}^2 M_{IA} = 0 \quad \ldots\ldots\ldots\ldots\ldots\ldots \text{(A-6)}$$

where $\theta = \theta_1 = \theta_2 = \theta_3 = \theta_4$ { because $\sin^2\theta_i = \sin^2\theta$ and $\cos^2\theta_i = \cos^2\theta$ due to assumed symmetry

$$M_{IA} = m\left[(R/r - 1)R/r + (\rho/r)^2\right] \quad \ldots\ldots\ldots\ldots\ldots\ldots \text{(A-7)}$$

Since the vertical and yaw axes (equations (A-3) and (A-6)) are completely uncoupled, tune these directions first and then see how the remaining equations might be satisfied. First, the vertical tuning requirement is

$$K_v = \omega_A^2 \, m\left[(R/r - 1)\, R/r + (\rho/r)\right] = \omega_A^2 M_{IA} \quad \ldots\ldots \quad \text{(A-3a)}$$

The isolation frequency, ω_A, is predetermined, 4/rev at 425 RPM = 28.3 Hz for the BO-105. Thus the only parameters (in equation A-3a) which may be traded off against each other are the vertical spring rate K_v, and the inertia bar properties of mass, m, inertia, $\rho^2 m$, and its C.G. location relative to the pivots, R/r. Assuming that the numerical values of these parameters are given, the yaw tuning requirement is obtained by rewriting equation (A-6) as

$$K_\tau \frac{\ell_s^2}{(\ell_x + r)\ell_x} = \omega_A^2 M_{IA} \quad \ldots\ldots\ldots\ldots\ldots\ldots \quad \text{(A-6a)}$$

If the same inertial bar is used in the tangential direction as in the vertical direction above, the values on the right hand side of the equation have already been preselected, and therefore the tangential tuning is <u>not</u> independent of the vertical spring rate. Equating the left hand sides of the two tuning equations gives

$$K_\tau \frac{\ell_s^2}{(\ell_x + r)\ell_x} = K_v \quad \ldots\ldots\ldots \quad \text{(A-8)}$$

For coincident tuning in the vertical and yaw directions, the tangential and vertical spring rates are not independent but related by the geometric locations of the transmission pivot, ℓ_x, fuselage pivot, $\ell_x + r$, and main spring attachment to fuselage ℓ_s.

Considering the pitch direction, two relations have to be satisfied. The first is

$$K_v \frac{\ell_s^2}{(\ell_x + r)\ell_x} = \omega_A^2 M_{IA} \quad \ldots\ldots\ldots\ldots\ldots\ldots \quad \text{(A-5a)}$$

Substituting from equation (A-3a) for the r/h side yields

$$K_v \frac{\ell_s^2}{(\ell_x + r)\ell_x} = K_v$$

or

$$\frac{\ell_s^2}{(\ell_x + r)\ell_x} = 1 \quad \ldots\ldots\ldots\ldots\ldots\ldots\ldots\ldots \text{(A-9)}$$

This relation states that for concurrent pitch and vertical tuning the spring attachment to the fuselage must be located between the transmission pivot and the fuselage pivot.

Substituting equation (A-9) into equation (A-8) results in

$$K_\tau = K_v \quad \ldots\ldots\ldots\ldots\ldots\ldots\ldots\ldots \text{(A-10)}$$

The second condition which must be satisfied in pitch appears also in the longitudinal direction

$$(K_\tau - \omega_A^2 M_{IA}) \cos^2\theta + K_r \sin^2\theta = 0 \quad \ldots\ldots\ldots\ldots \text{(A-1a)}$$

The coefficient of $\cos^2\theta$ is zero by equations (A-10) and (A-3) leaving

$$K_r \sin^2\theta = 0 \quad \ldots\ldots\ldots\ldots\ldots\ldots\ldots\ldots \text{(A-11)}$$

Considering the lateral tuning requirement

$$(K_\tau - \omega_A^2 M_{IA}) \sin^2\theta + K_r \cos^2\theta = 0 \quad \ldots\ldots\ldots\ldots \text{(A-2a)}$$

the same reasoning leads to

$$K_r \cos^2\theta = 0 \quad \ldots\ldots\ldots\ldots\ldots\ldots\ldots\ldots \text{(A-12)}$$

The only solution satisfying equations (A-11) and (A-12) simultaneously is

$$K_r = 0 \quad \ldots\ldots\ldots\ldots\ldots\ldots\ldots\ldots\ldots\ldots \text{(A-13)}$$

Roll tuning will be achieved automatically if pitch tuning is attained.

In order to accomplish coincident tuning in 6-axes, at $\omega = \omega_A$ the following relations must be satisfied:

$$\left.\begin{aligned} K_v &= \omega_A{}^2 m \left[(R/r - 1)\, R/r + (\rho/r)^2 \right] \\ K_\tau &= K_v \\ K_r &= 0 \\ \ell_s{}^2 &= (\ell_x + r)\ell_x \end{aligned}\right\} \quad \ldots\ldots\ldots \quad (A\text{-}14)$$

APPENDIX B

EQUATIONS OF MOTION

The equations of motion in matrix form are shown below.

$$\underset{12x12}{\left[-\left[A\right]\eta^2 + \left[C\right]\right]} \underset{1x12}{\left\{q\right\}} = \frac{1}{M_x \Omega^2} \underset{1x12}{\left\{F\right\}} \quad \ldots\ldots\ldots (B\text{-}1)$$

where $\eta = \omega/\Omega$ forcing frequency/rotor speed ratio

$M_x \sim$ transmission mass

$\Omega \sim$ rotor speed

$$\left[A\right] = \left[A_{XMSN/FUS}\right] + \left[A_{BARS}\right] \quad \ldots\ldots\ldots\ldots\ldots\ldots (B\text{-}2)$$

$\left[A_{XMSN/FUS}\right] \sim$ see equation (B-5)

$$\left[A_{BARS}\right] = \sum_{i=1}^{4} \frac{m_i}{M_x} \underset{3x12}{\left[L\right]_i^T} \underset{3x3}{\begin{bmatrix} 1 & & \\ & 1 & \\ & & 1 \end{bmatrix}} \underset{12x3}{\left[L\right]_i}$$

$$+ \left(\frac{\rho}{r}\right)^2 \underset{2x12}{\left[R\right]_i^T} \underset{2x\ 2}{\begin{bmatrix} 1 & \\ & 1 \end{bmatrix}} \underset{12x2}{\left[R\right]_i} \quad \ldots\ldots\ldots\ldots\ldots (B\text{-}3)$$

$m_i \sim$ IRIS inertia bar weight

$L_i \sim$ see equation (B-8)

$R_i \sim$ see equation (B-9)

$\rho \sim$ inertia bar radius of gyration

$r \sim$ pivot separation

$$\left\{q\right\}^T = \left\{x_x,\ y_x,\ z_x,\ \alpha_x,\ \beta_x,\ \gamma_x,\ x_F,\ y_F,\ z_F,\ \alpha_F,\ \beta_F,\ \gamma_F\right\}$$

$$\underset{12x3}{\left[C\right]} = \sum_{ix1}^{4} \underset{12x3}{\left[D\right]_i^T} \begin{bmatrix} \frac{K_\tau}{M_x \Omega^2} & & \\ & \frac{K_r}{M_x \Omega^2} & \\ & & \frac{K_v}{M_x \Omega^2} \end{bmatrix}_{3x3} \underset{3x12}{\left[D\right]_i} \quad \ldots \quad (B\text{-}4)$$

D_i ∿ see equation (B-10)

K_τ ∿ tangential spring rate, one IRIS unit

K_r ∿ radial spring rate, one IRIS unit

K_v ∿ vertical spring rate, one IRIS unit

$$\left[A_{XMSN/FUS}\right] = \left[\begin{array}{c|c} A_x & \\ \hline & A_F \end{array}\right] \left\{q\right\} \quad \text{. . . . .(B-5)}$$

$$\left[A_x\right] = \begin{bmatrix} 1 & & & & & \\ & 1 & & & & \\ & & 1 & & & \\ & & & k_{x\alpha} & & \\ & & & & k_{x\beta} & \\ & & & & & k_{x\gamma} \end{bmatrix} \begin{matrix} x_x \\ y_x \\ z_z \\ \alpha_x \\ \beta_x \\ \gamma_x \end{matrix}$$

. . . .(B-6)

$$\left[A_F\right] = \begin{bmatrix} 1 & & & & & \\ & 1 & & & & \\ & & 1 & & & \\ & & & M_5 k_{F\alpha}^2 & & \\ & & & & M_5(k_{F\beta}^2 + X_G^2) & \\ & & & & & M_5(k_{F\gamma}^2 + X_G^2) \end{bmatrix} \begin{matrix} x_F \\ y_F \\ z_F \\ \alpha_F \\ \beta_F \\ \gamma_F \end{matrix}$$

. . . .(B-7)

$$
\left[L \right]_i^T =
\begin{array}{c}
\begin{array}{ccc} \text{TANGENTIAL} & \text{RADIAL} & \text{VERTICAL} \end{array} \\
\left[\begin{array}{ccc}
(R_r - 1)\cos\theta_i & \sin\theta_i & 0 \\
(R_r - 1)\sin\theta_i & \cos\theta_i & 0 \\
0 & 0 & -(R_r - 1) \\
-h_x(R_r - 1)\sin\theta_i & -h_x\cos\theta_i & \ell_x(R_r - 1)\cos\theta_i \\
-h_x(R_r - 1)\cos\theta_i & h_x\sin\theta_i & -\ell_x(R_r - 1)\sin\theta_i \\
-\ell_x(R_r - 1) & 0 & 0 \\
R_r\cos\theta_i & 0 & 0 \\
-R_r\sin\theta_i & 0 & 0 \\
0 & 0 & R_r \\
-h_F R_r\sin\theta_i & 0 & -(\ell_x + r)R_r\cos\theta_i \\
-h_F R_r\cos\theta_i & 0 & (\ell_x + r)R_r\sin\theta_i \\
(\ell_x + r)R_r & 0 & 0
\end{array}\right]
\end{array}
\begin{array}{l}
x_X \\ y_X \\ z_X \\ \alpha_X \\ \beta_X \\ \gamma_X \\ x_F \\ y_F \\ z_F \\ \alpha_F \\ \beta_F \\ \gamma_F
\end{array}
\qquad \ldots\ldots (B\text{-}8)
$$

LINEAR MOTION MATRIX OF i^{TH} INERTIA BAR

$$
\left[R \right]_i^T = \begin{array}{c} \tau \\ \text{TANGENTIAL} \end{array} \quad \begin{array}{c} V \\ \text{VERTICAL} \end{array}
$$

$$
\left[R \right]_i^T = \left[\begin{array}{cc} -\cos\theta_i & 0 \\ \sin\theta_i & 0 \\ 0 & 1 \\ -h_x \sin\theta_i & -\ell_x \cos\theta_i \\ -h_x \cos\theta_i & \ell_x \sin\theta_i \\ -\ell_x & 0 \\ \hline \cos\theta_i & 0 \\ -\sin\theta_i & 0 \\ 0 & -1 \\ -h_F \sin\theta_i & (\ell_x + r)\cos\theta_i \\ -h_F \cos\theta_i & -(\ell_x + r)\sin\theta_i \\ \ell_x + r & 0 \end{array} \right] \begin{array}{c} x_x \\ y_x \\ z_x \\ \alpha_x \\ \beta_x \\ \gamma_x \\ \hline x_F \\ y_F \\ z_F \\ \alpha_F \\ \beta_F \\ \gamma_F \end{array} \qquad \text{(B-9)}
$$

ROTATIONAL MOTION MATRIX OF i^{TH} INERTIA BAR

$$
\begin{matrix}
 & K_T & K_r & K_v & \\
\left[\ D\ \right]_i^T = & \left[\begin{array}{ccc}
\cos\theta_i & -\sin\theta_i & 0 \\
-\sin\theta_i & -\cos\theta_i & 0 \\
0 & 0 & 1 \\
h_x\sin\theta_i & h_x\cos\theta_i & -\ell_s\cos\theta_i \\
h_x\cos\theta_i & -h_x\sin\theta_i & \ell_s\sin\theta_i \\
\ell_s & 0 & 0 \\
\hline
-\cos\theta_i & \sin\theta_i & 0 \\
\sin\theta_i & \cos\theta_i & 0 \\
0 & 0 & -1 \\
h_F\sin\theta_i & h_F\cos\theta_i & \ell_s\cos\theta_i \\
h_F\cos\theta_i & -h_F\sin\theta_i & -\ell_s\sin\theta_i \\
-\ell_s & 0 & 0
\end{array}\right] & \begin{array}{c} x_x \\ y_x \\ z_x \\ \alpha_x \\ \beta_x \\ \gamma_x \\ \hline x_F \\ y_F \\ z_F \\ \alpha_F \\ \beta_F \\ \gamma_F \end{array}
\end{matrix}
\qquad \ldots\ldots\ldots \text{(B-10)}
$$

SPRING DEFLECTION MATRIX FOR i^{TH} IRIS UNIT

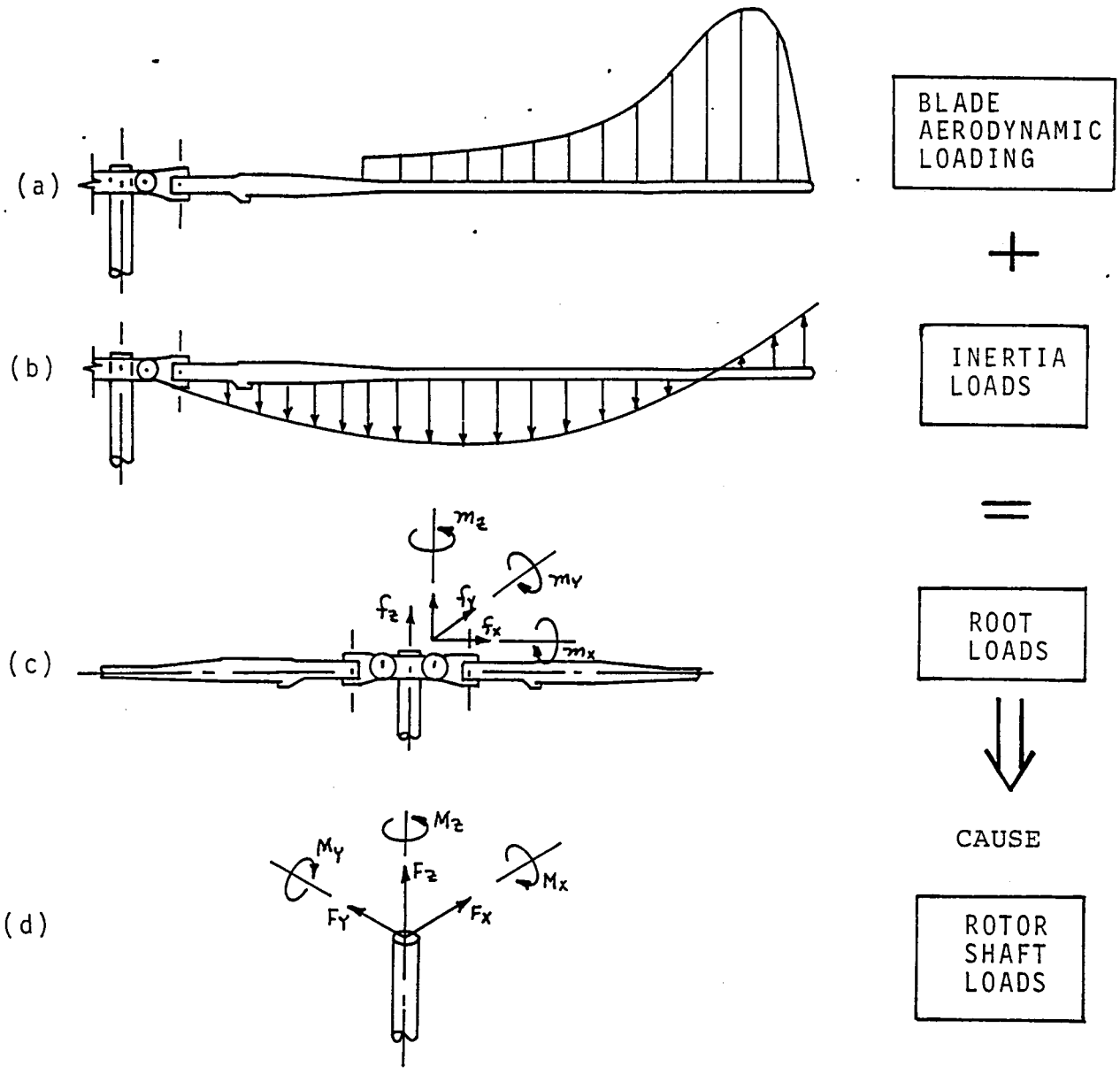

Figure 2.1 Sources of rotor loads

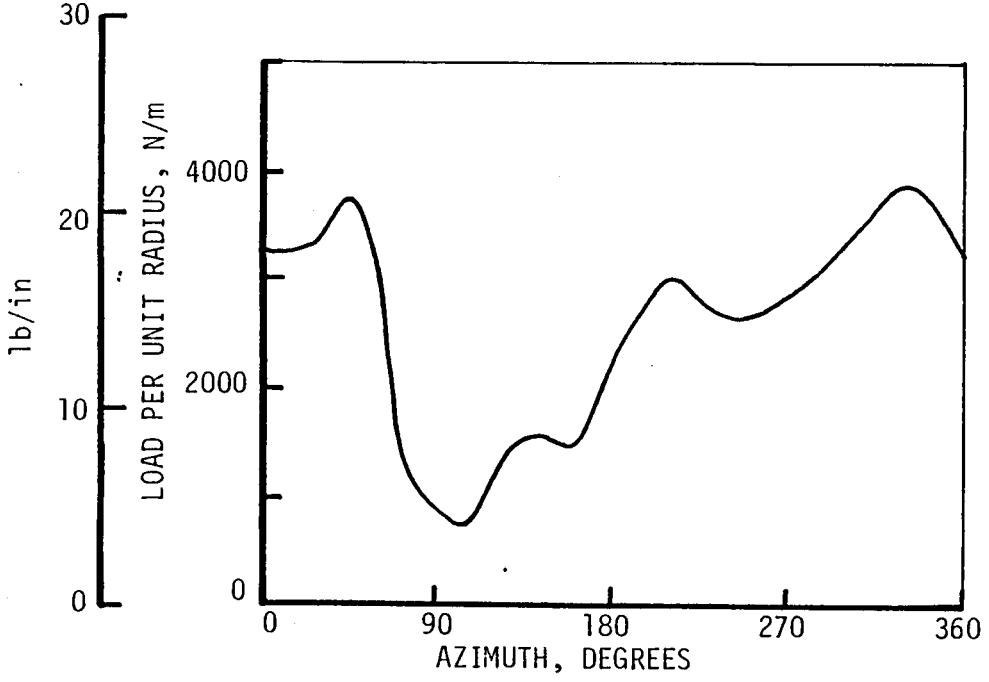

HARMONIC CONTENT		
HARMONIC	VALUE N/m	(lb/in)
1	1101	(6.29)
2	520	(2.97)
3	196	(1.12)
4	342	(1.95)
5	266	(1.52)
6	26	(0.15)
7	52	(0.30)
8	74	(0.42)
9	79	(0.45)
10	51	(0.29)

Figure 2.2 CH-46A azimuthal blade loads at 95% radius, 135 kts

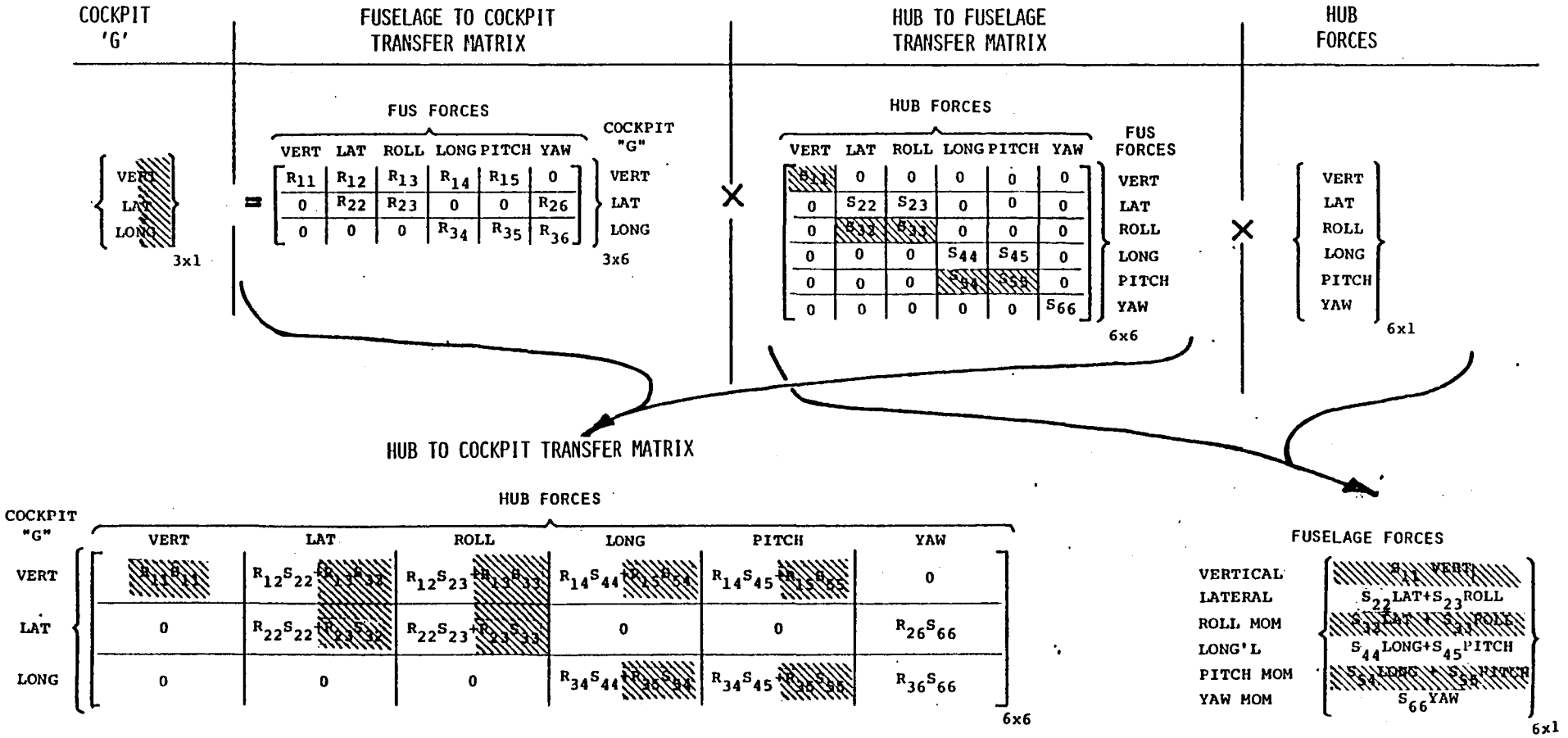

Figure 3.1-1 Relationship between cockpit vibration and hub forces

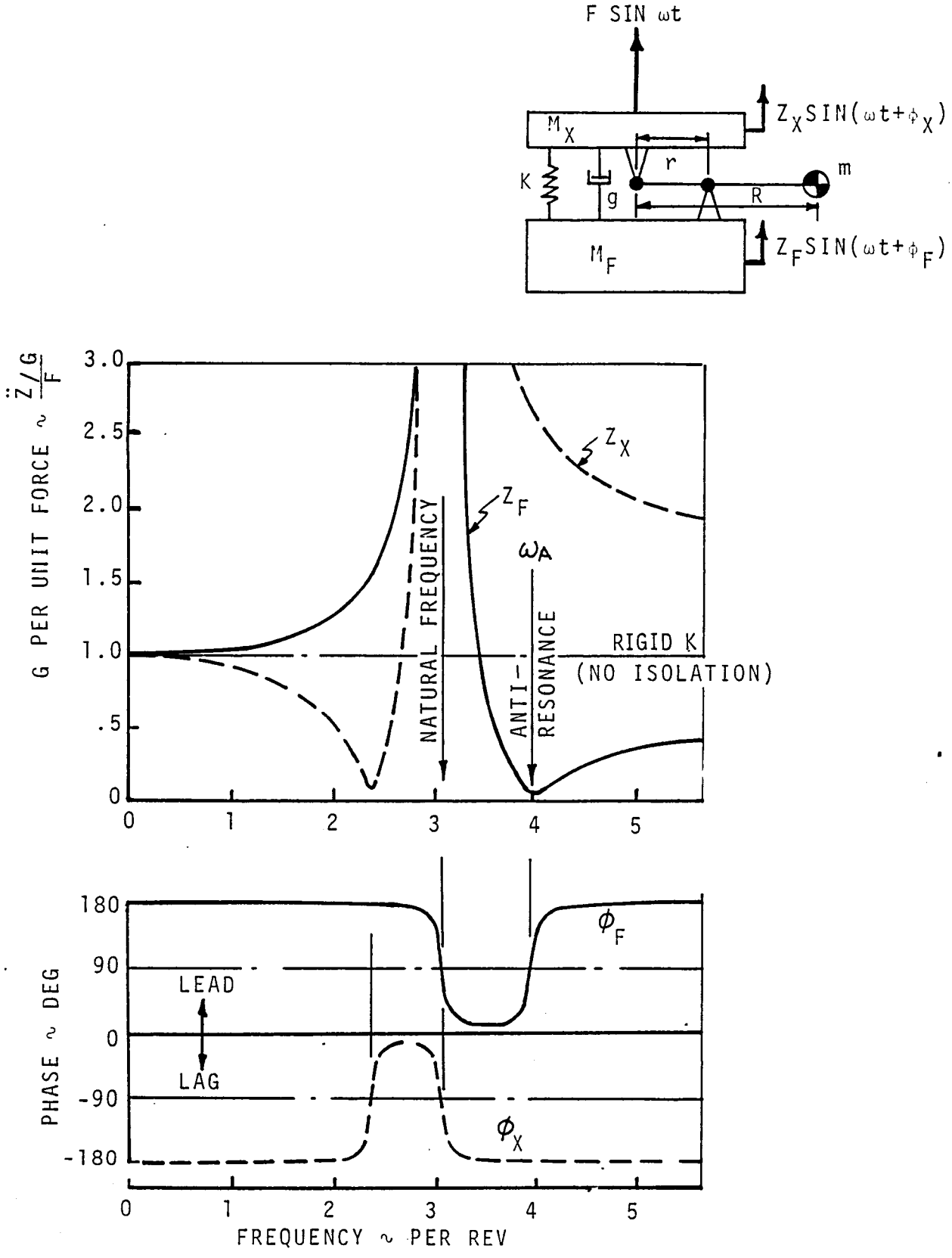

Figure 3.1-2 Basic antiresonant isolator characteristics

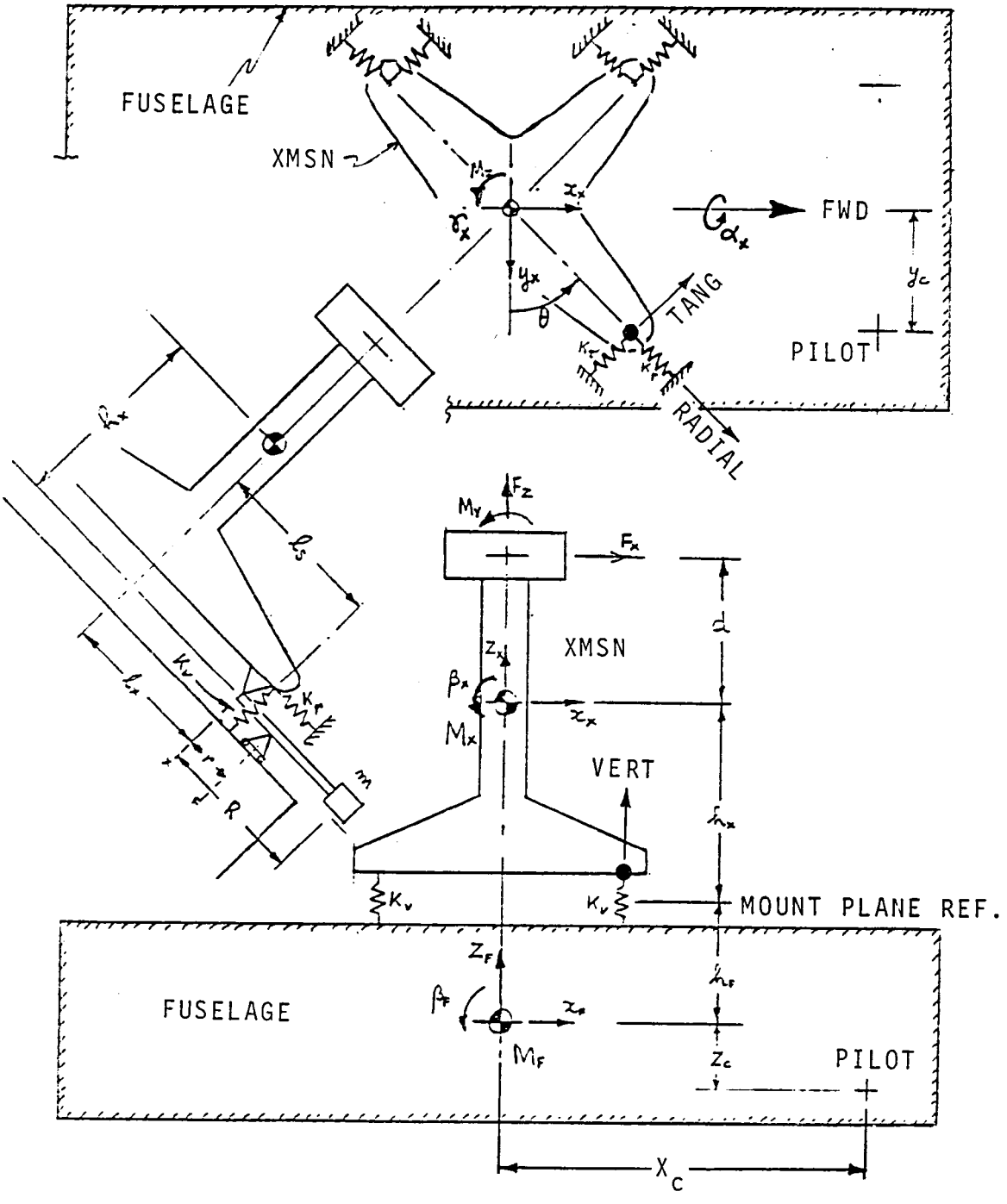

Figure 3.1-3 6 axis IRIS schematic

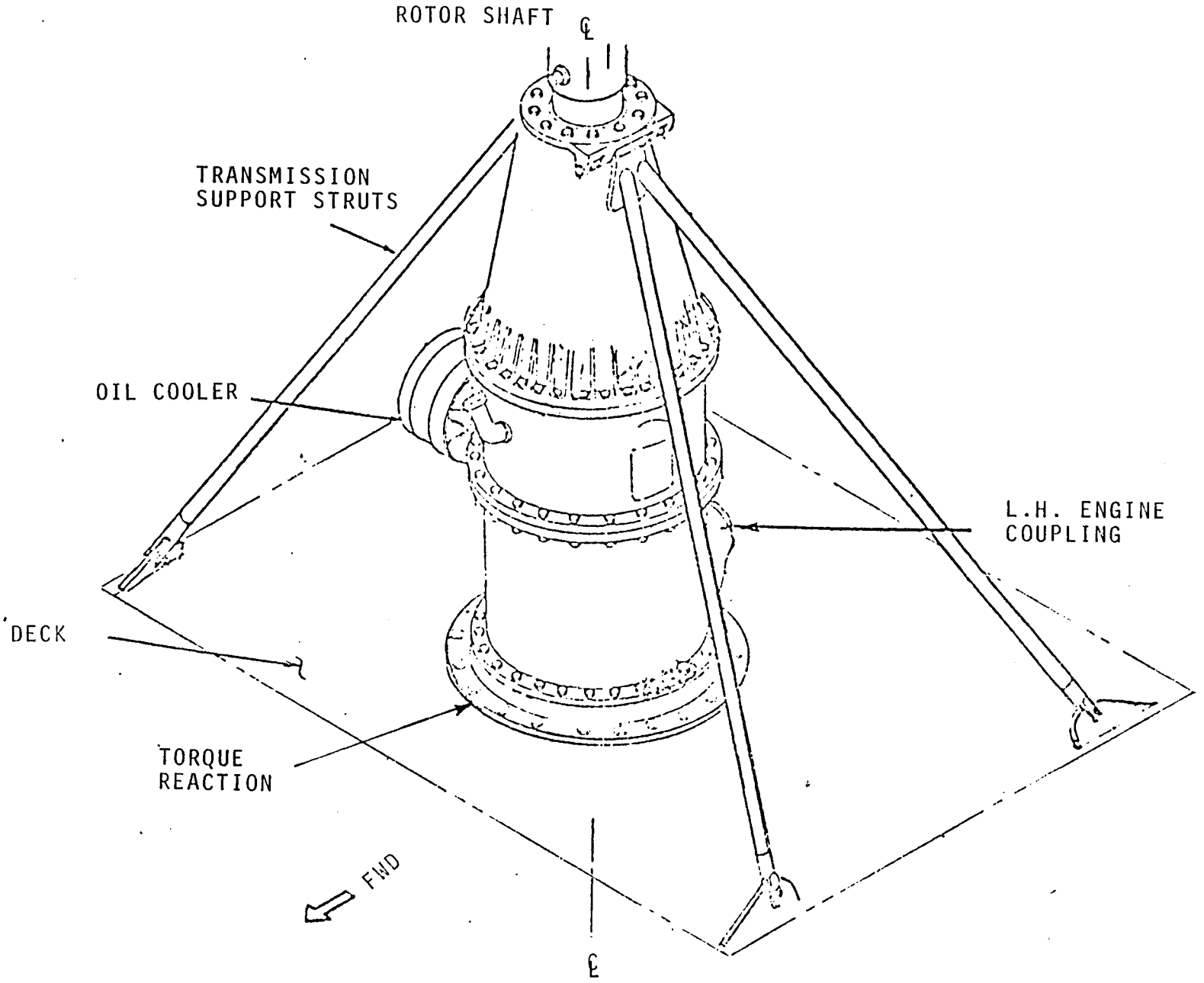

Figure 3.2-1 Standard installation of BO-105 transmission

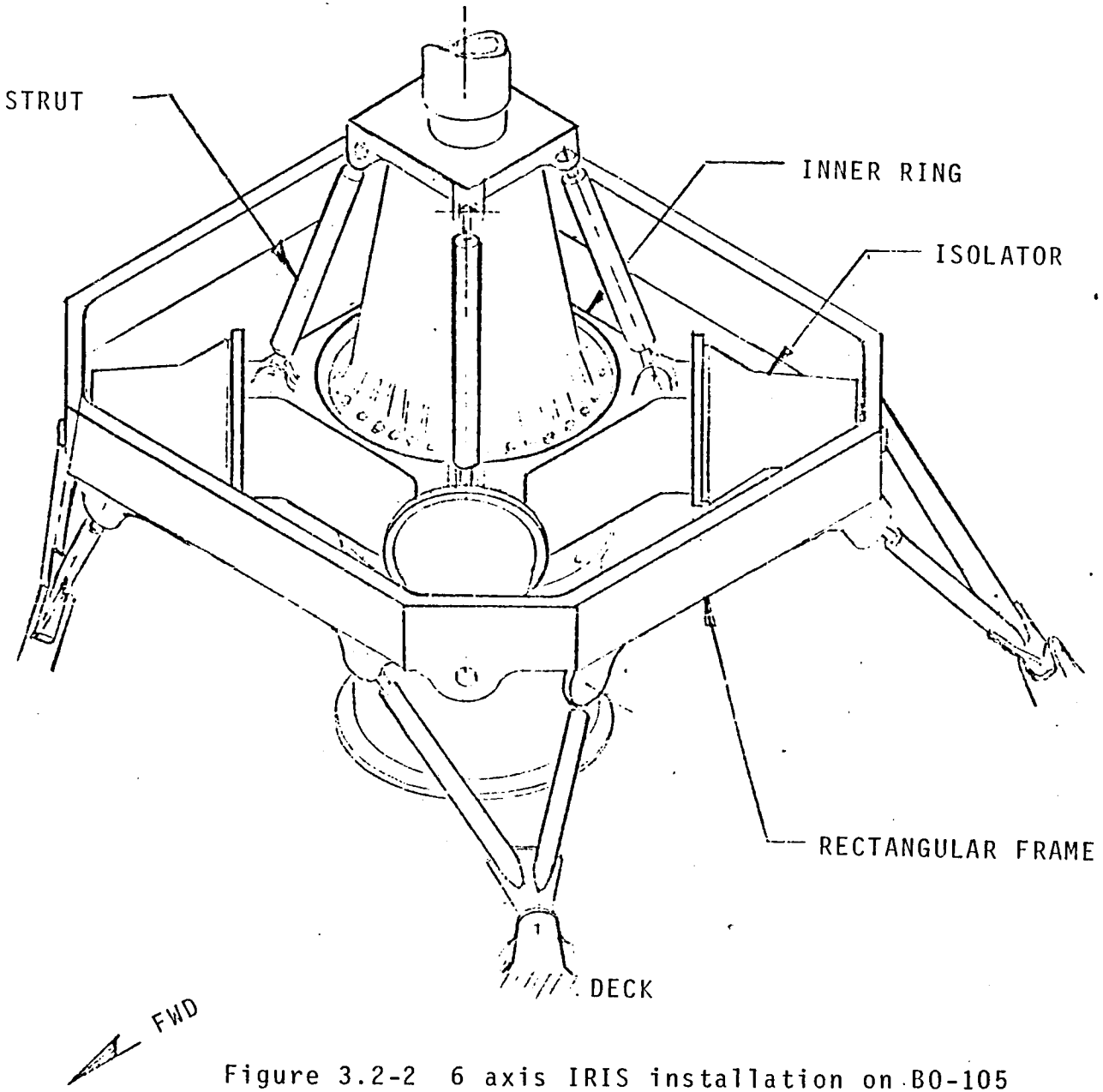

Figure 3.2-2 6 axis IRIS installation on BO-105

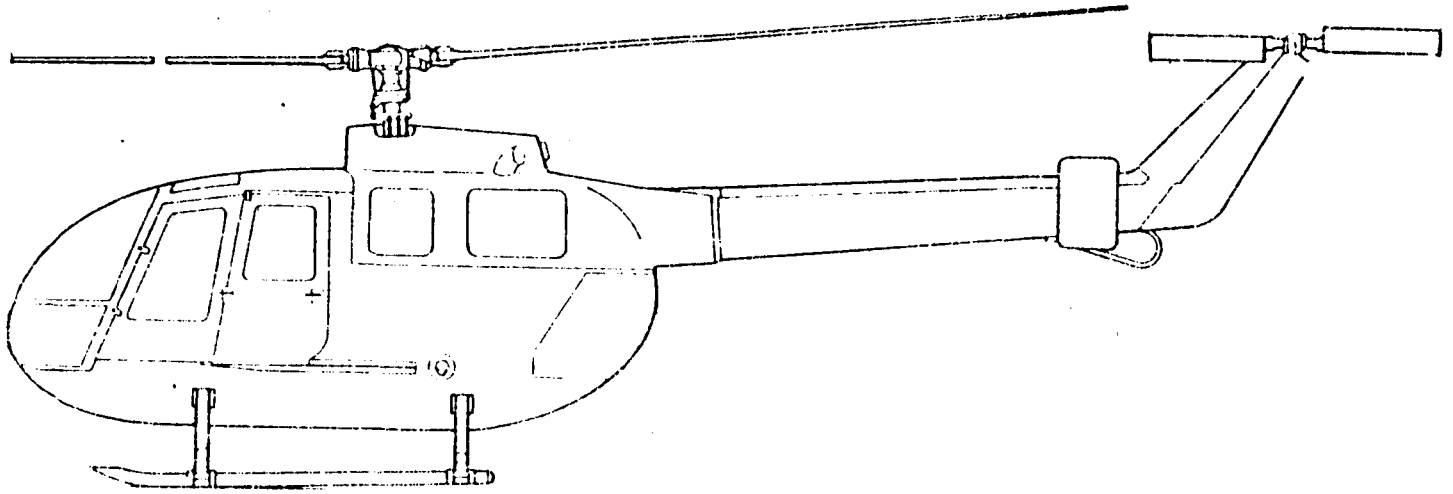

MISSION DGW: 2300 kg (5071 lb)

ROTOR SPEED: 424 RPM

NUMBER OF BLADES: 4

n/REV FREQUENCY: 28.3 HZ

Figure 3.2-3 BO-105 selected as baseline aircraft

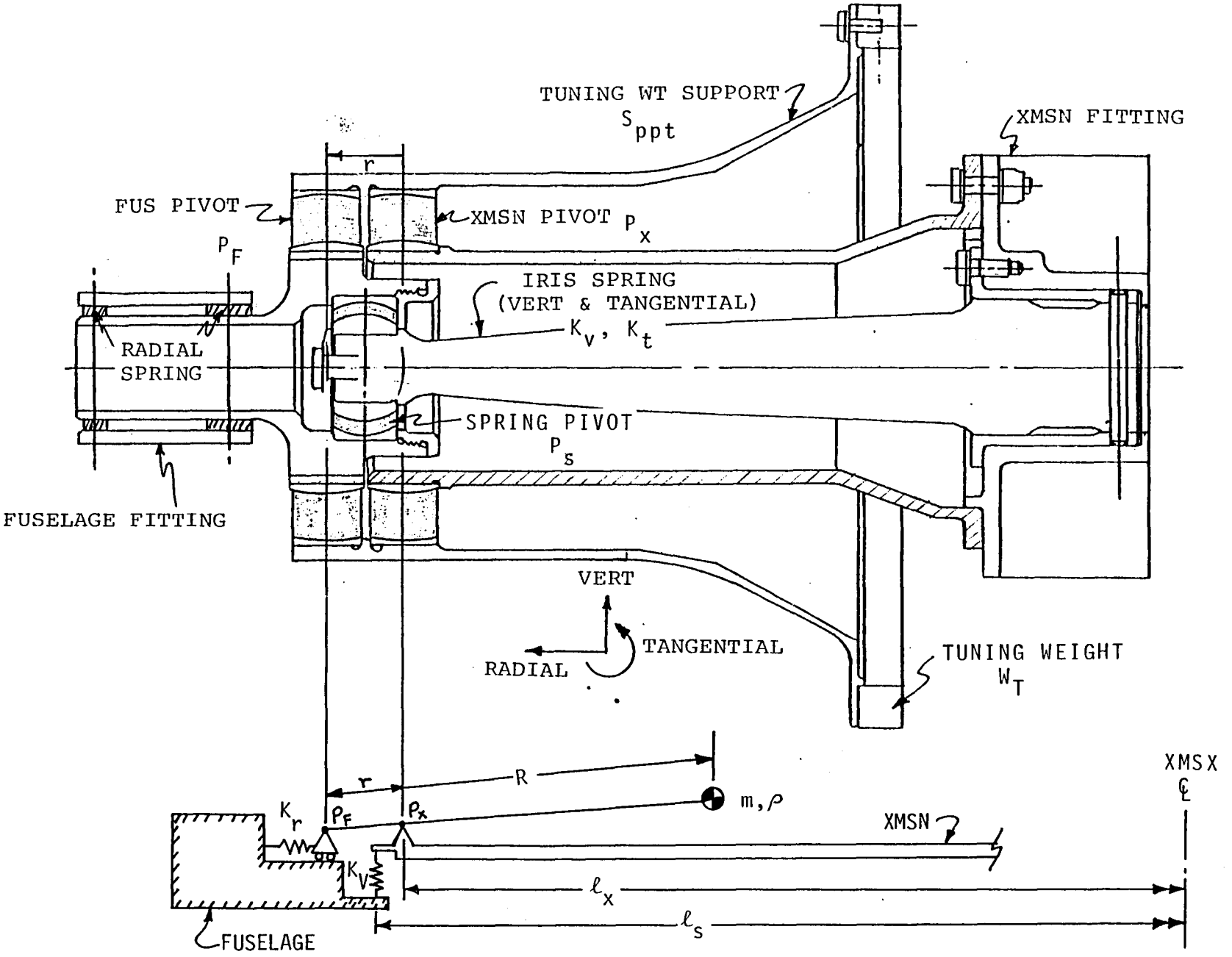

Figure ~~B3-1~~ Bidirectional IRIS unit

4

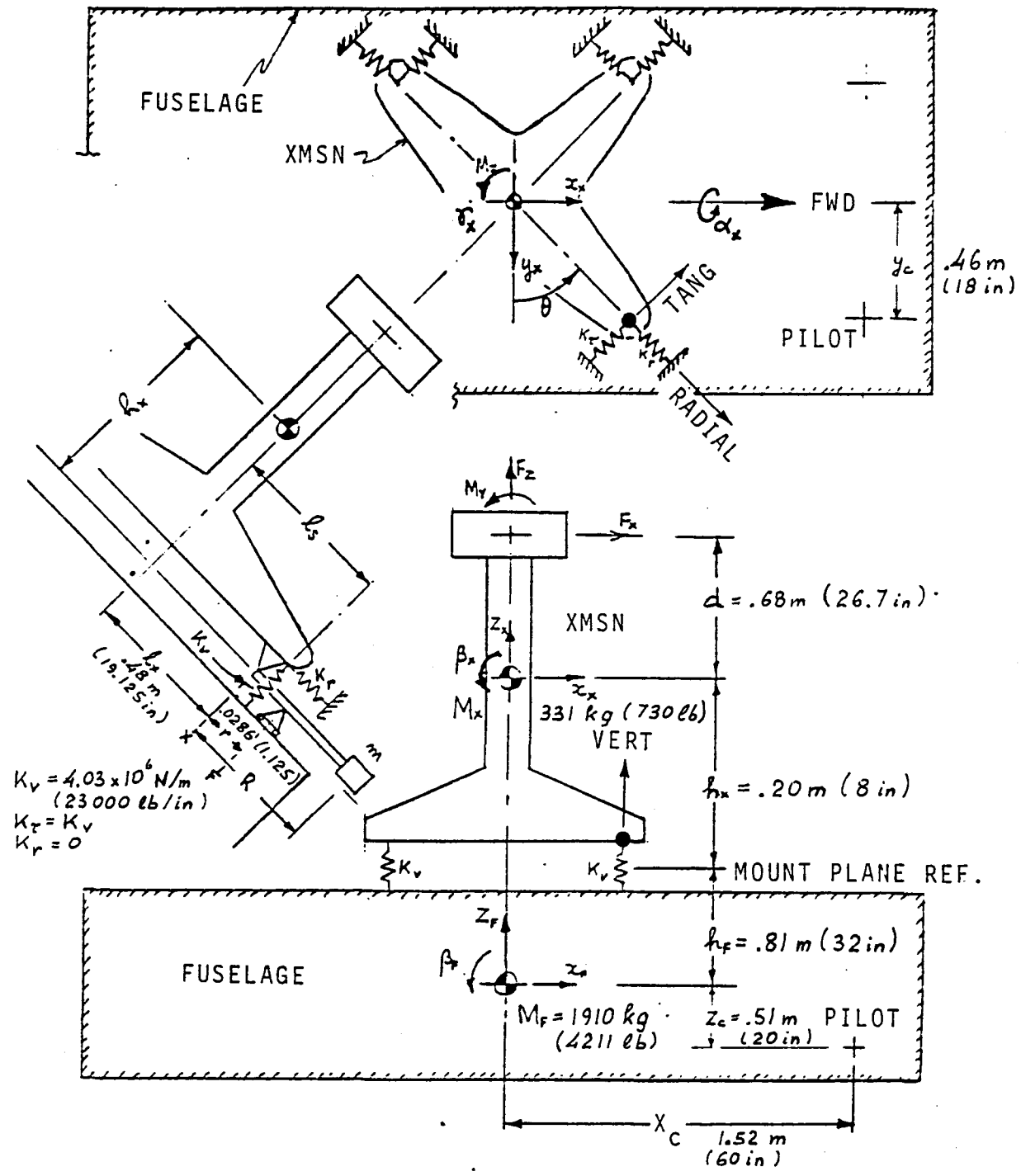

Figure 3.3-2 6 axis IRIS mathematical model
with physical properties of reference configuration

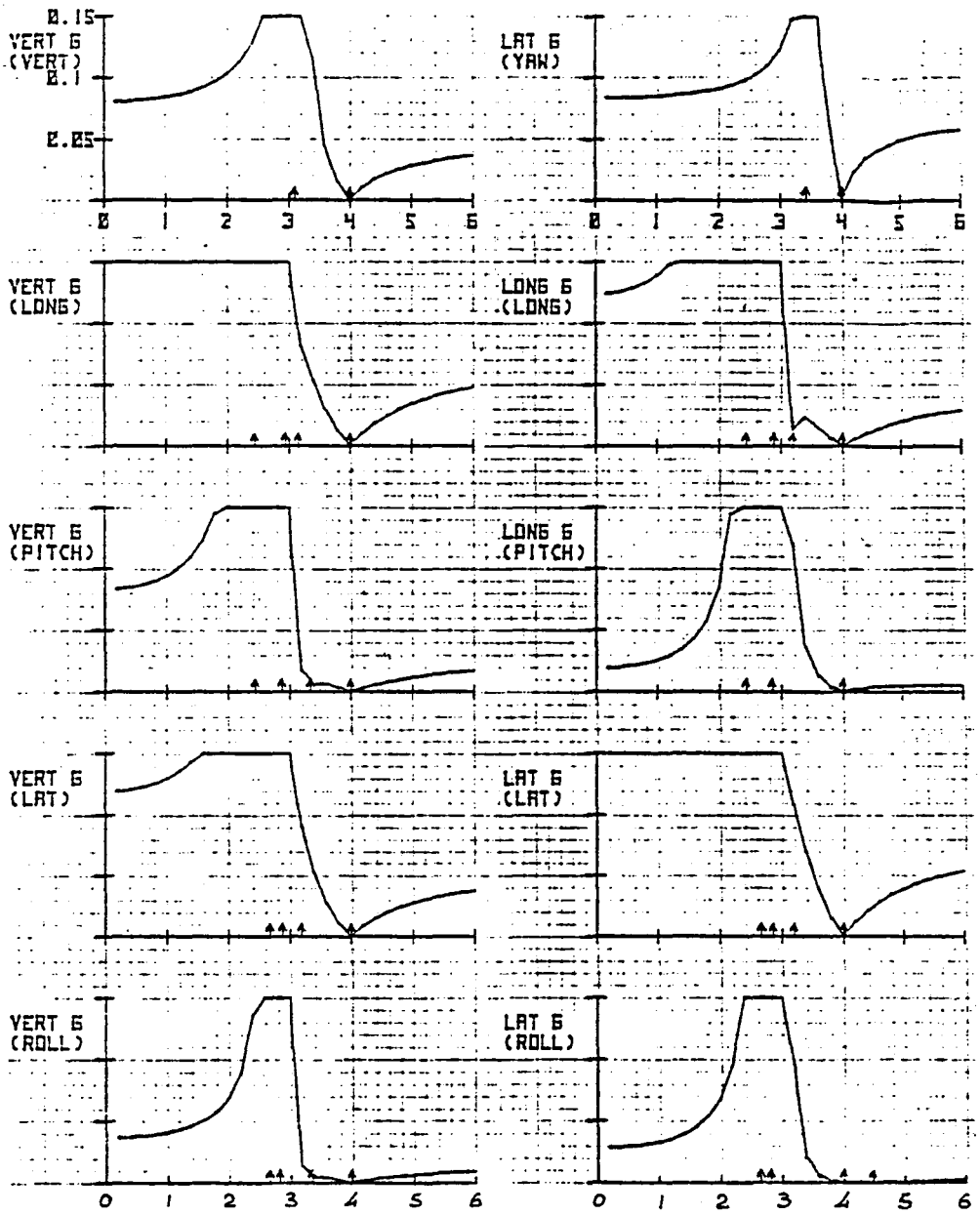

Figure 3.3-3 Cockpit response, reference configuration, K_r=0, 6 axis IRIS

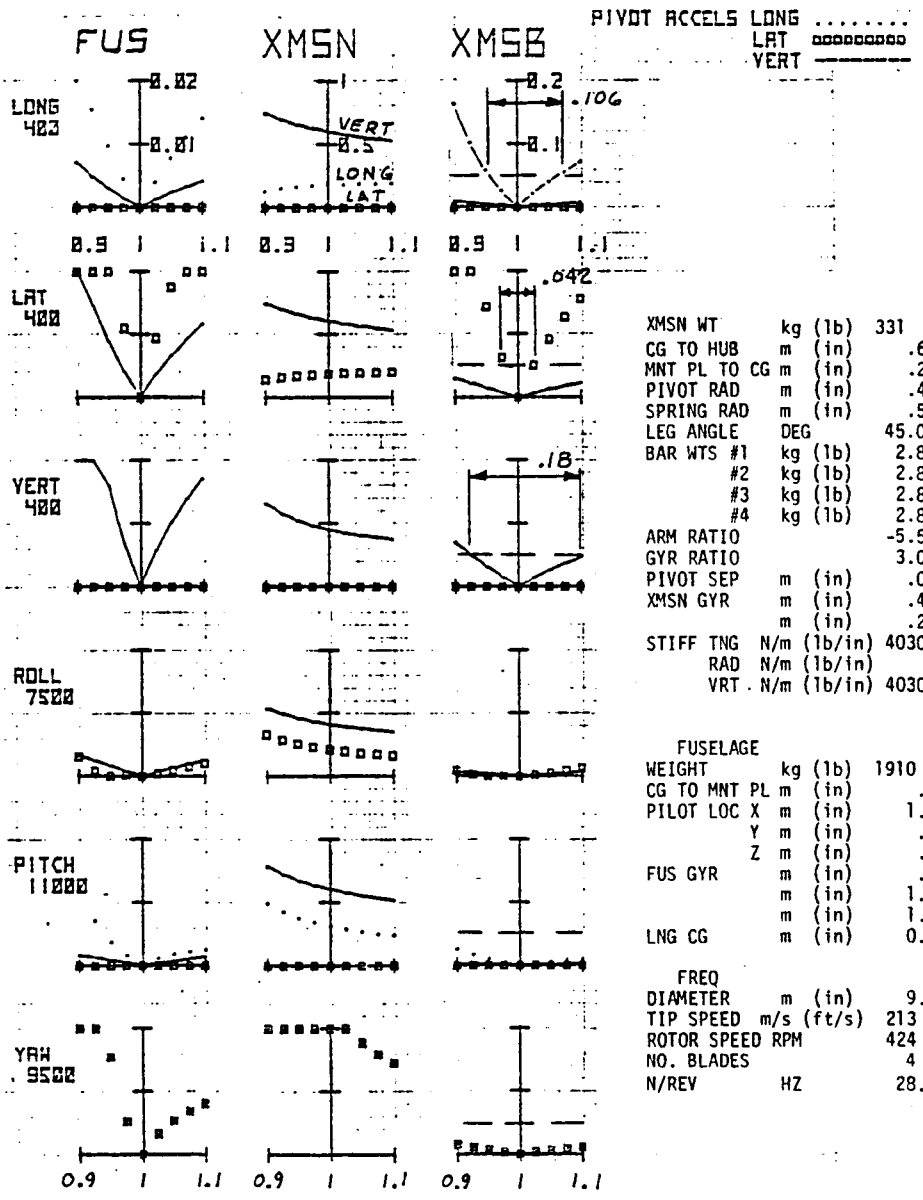

XMSN WT	kg	(lb)	331	(730)
CG TO HUB	m	(in)	.678	(26.7)
MNT PL TO CG	m	(in)	.203	(8)
PIVOT RAD	m	(in)	.486	(19.125)
SPRING RAD	m	(in)	.5	(19.68)
LEG ANGLE	DEG		45.0	
BAR WTS #1	kg	(lb)	2.81	(6.19)
#2	kg	(lb)	2.81	(6.19)
#3	kg	(lb)	2.81	(6.19)
#4	kg	(lb)	2.81	(6.19)
ARM RATIO			-5.56	
GYR RATIO			3.0	
PIVOT SEP	m	(in)	.0286	(1.125)
XMSN GYR	m	(in)	.453	(17.82)
	m	(in)	.254	(10)
STIFF TNG	N/m	(lb/in)	4030000	(23000)
RAD	N/m	(lb/in)	0	(0)
VRT	N/m	(lb/in)	4030000	(23000)

FUSELAGE				
WEIGHT	kg	(lb)	1910	(4211)
CG TO MNT PL	m	(in)	.813	(32)
PILOT LOC X	m	(in)	1.52	(60)
Y	m	(in)	.457	(18)
Z	m	(in)	.508	(20)
FUS GYR	m	(in)	.610	(24)
	m	(in)	1.02	(40)
	m	(in)	1.02	(40)
LNG CG	m	(in)	0.	(0)

FREQ				
DIAMETER	m	(in)	9.61	(378)
TIP SPEED	m/s	(ft/s)	213	(700)
ROTOR SPEED	RPM		424	
NO. BLADES			4	
N/REV	HZ		28.3	

FREQUENCY - PER REV/4

Figure 3.3-4 Fuselage/XMSN interface, response near 4/rev reference configuration, K_r=0, 6 axis IRIS

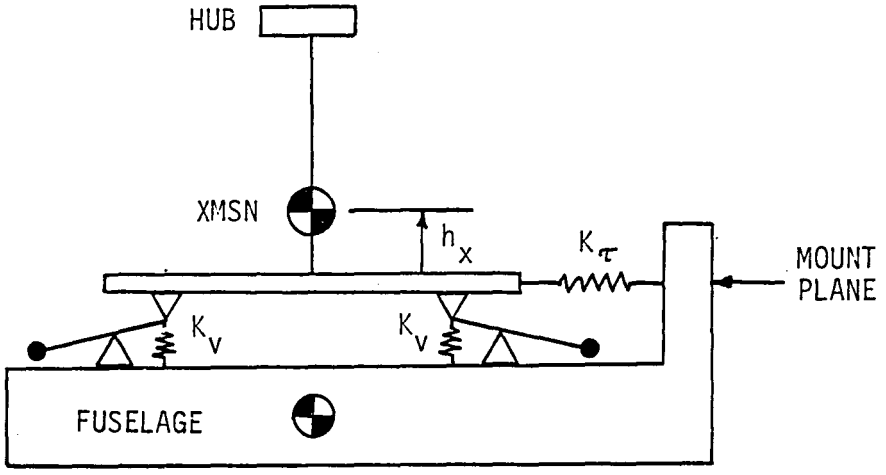

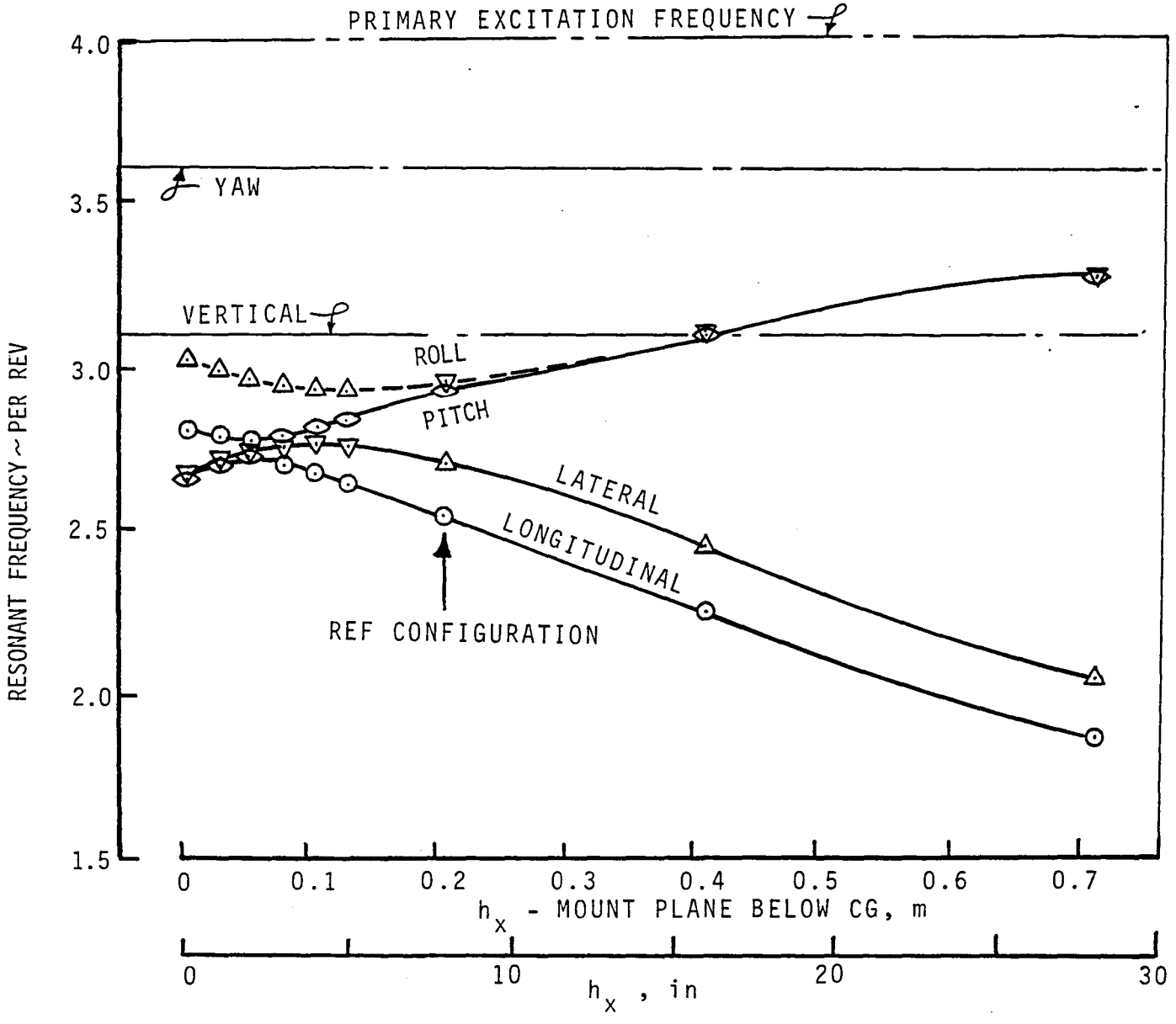

Figure 3.3-5 Mount plane effects on system resonances

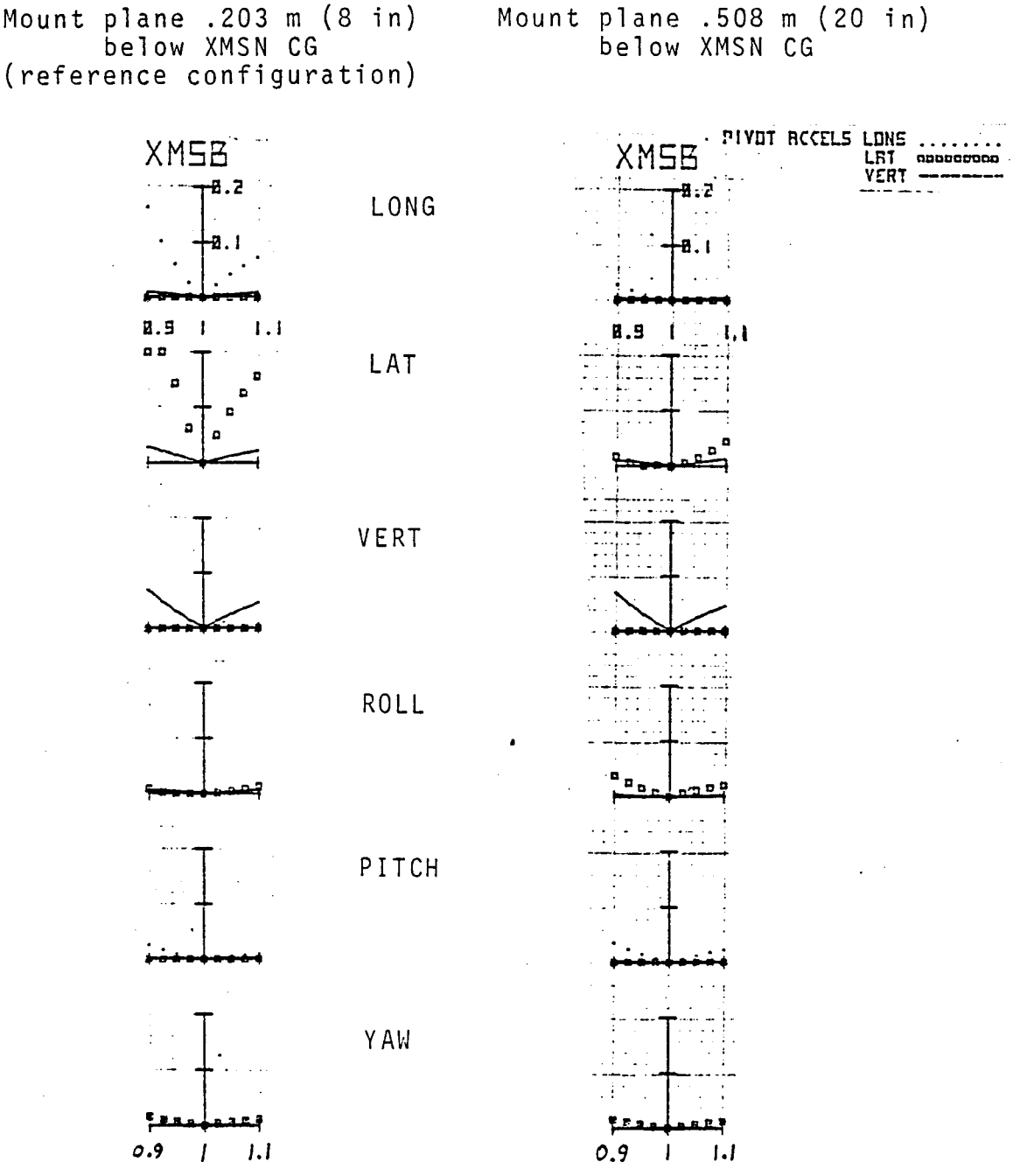

Figure 3.3-6 Mount plane effect on IRIS transmissibilities

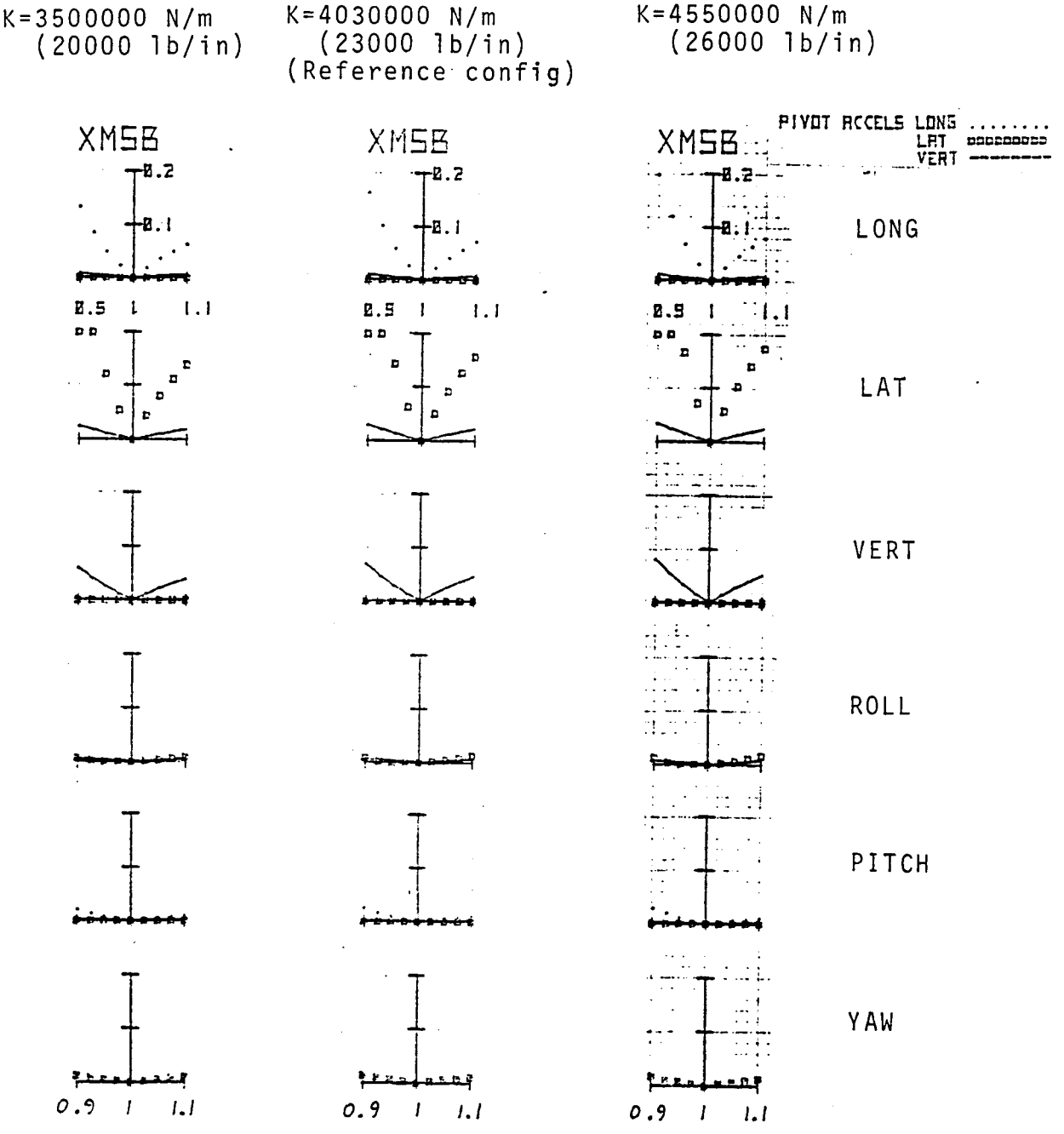

Figure 3.3-7 Spring rate effect on IRIS transmissibilites

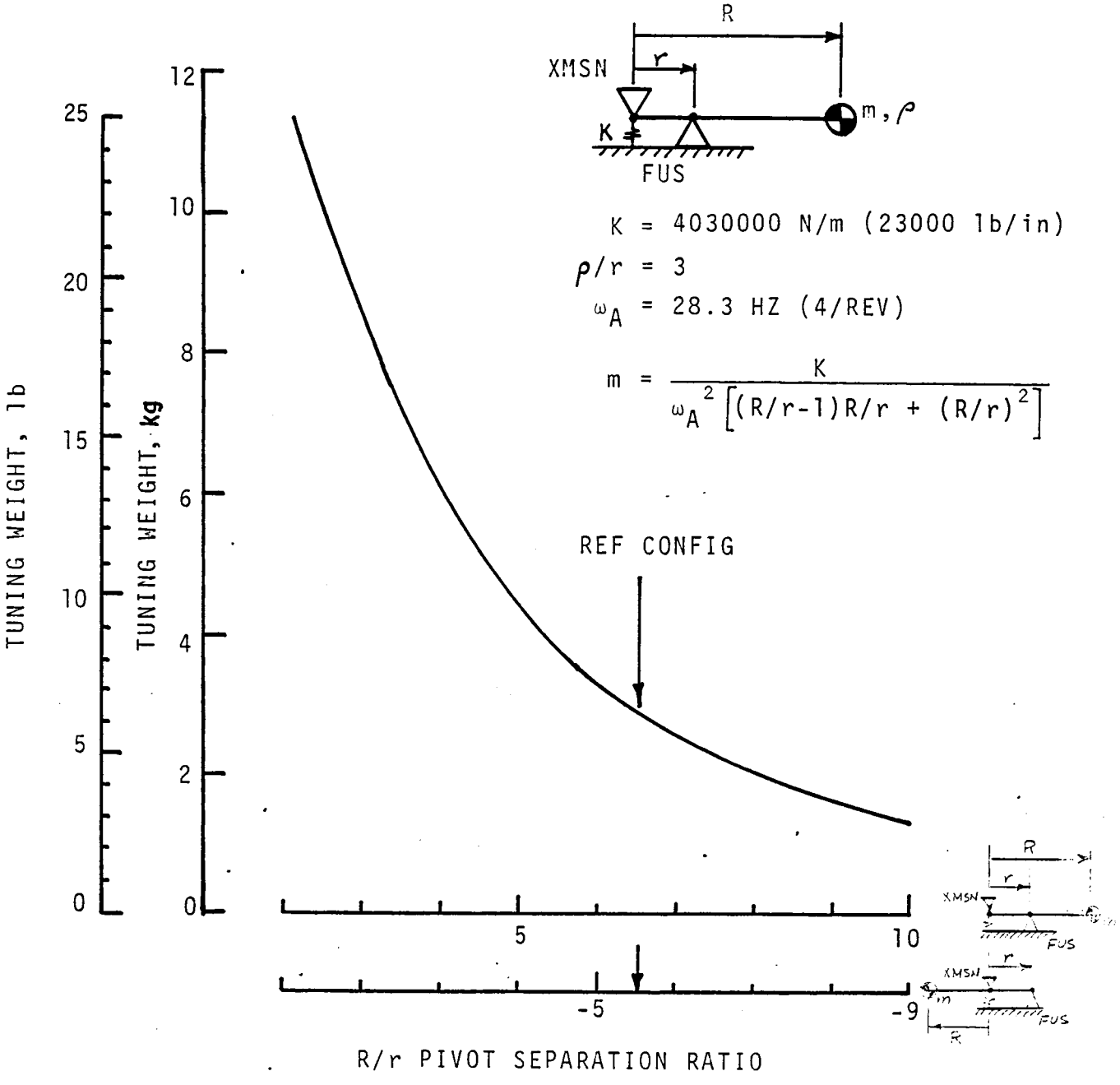

Figure 3.3-8 Effect of geometry on bar weight

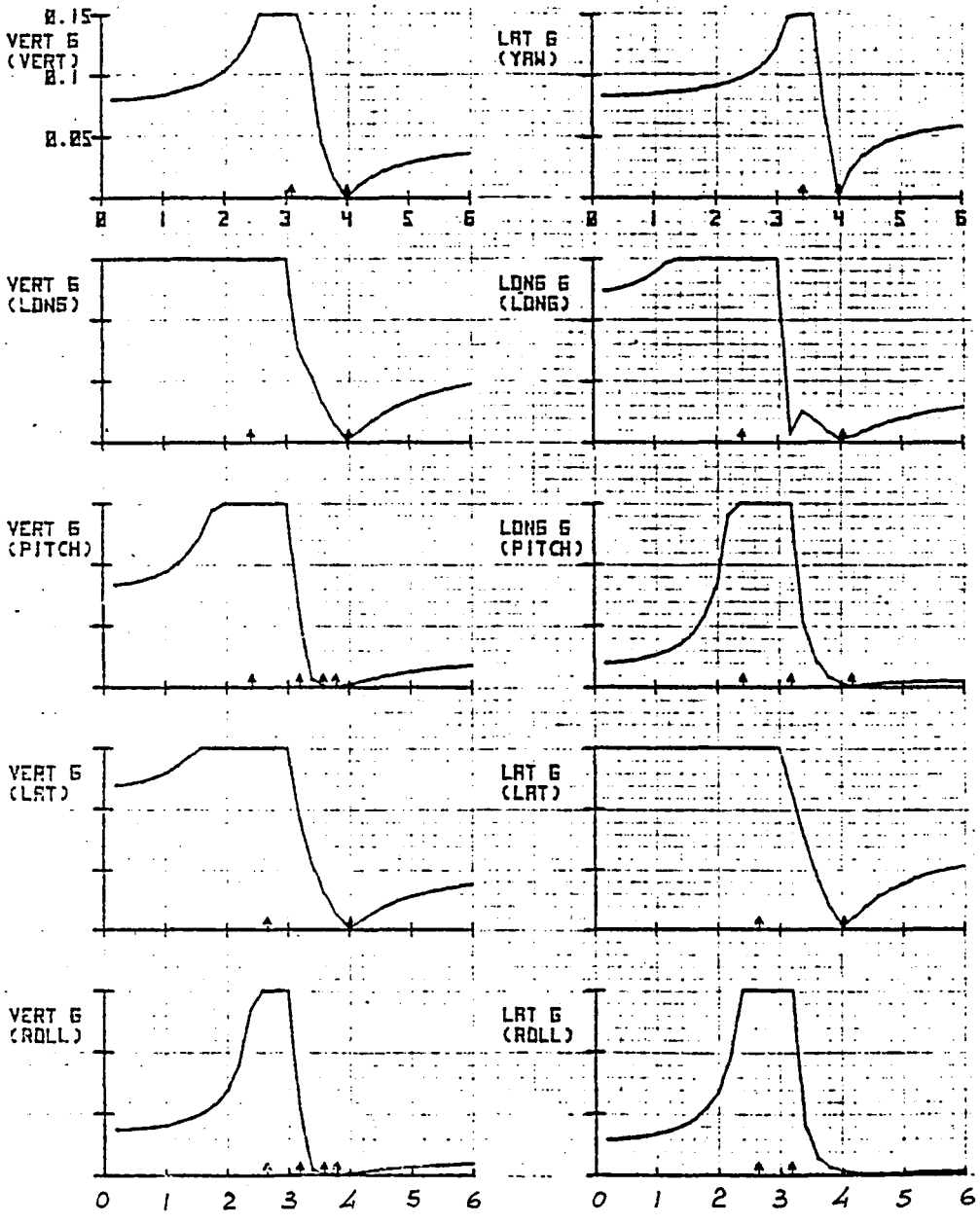

Figure 3.3-9 Cockpit response with non-zero radial spring rate

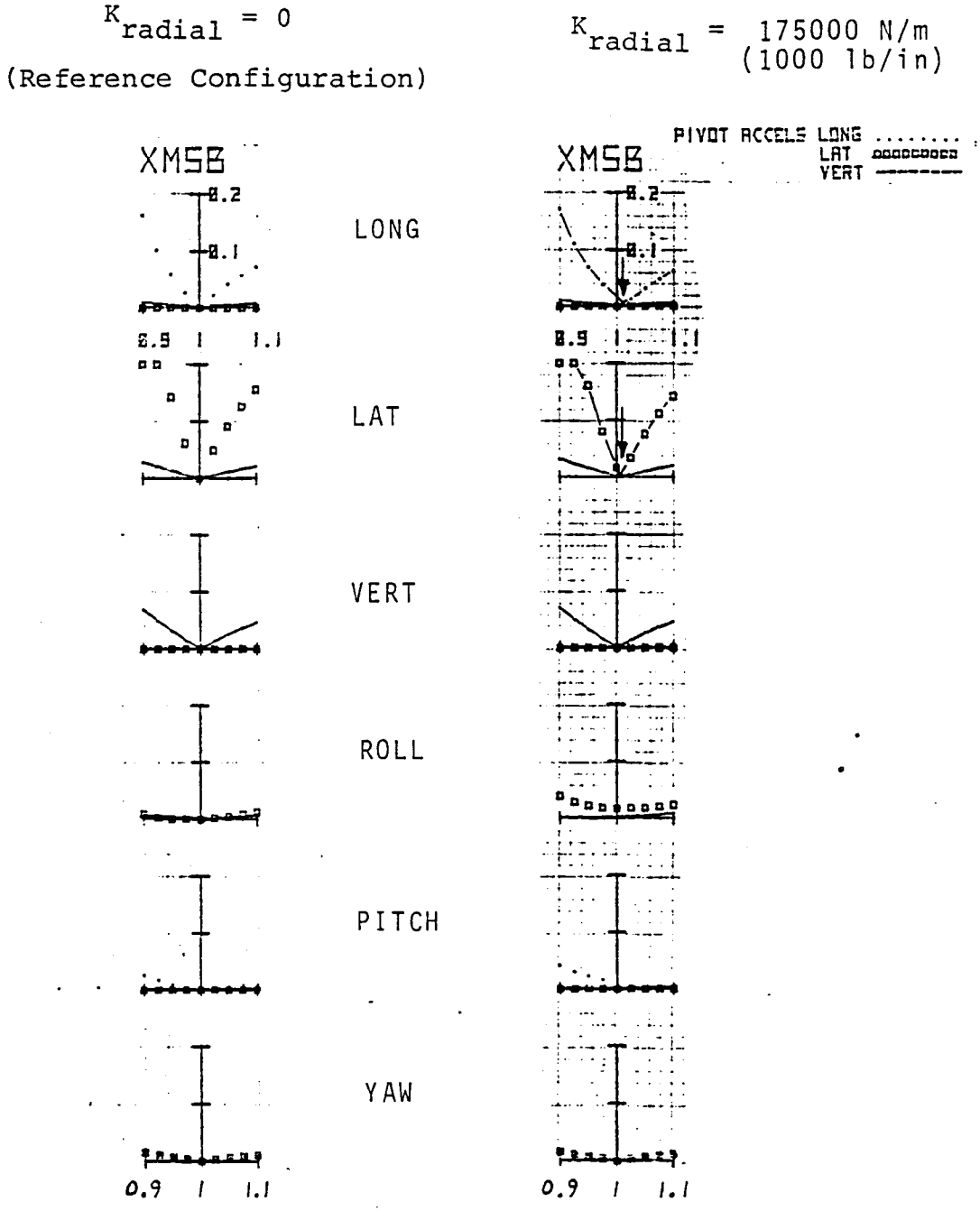

Figure 3.3-10 Transmissibilites with non-zero radial spring rate

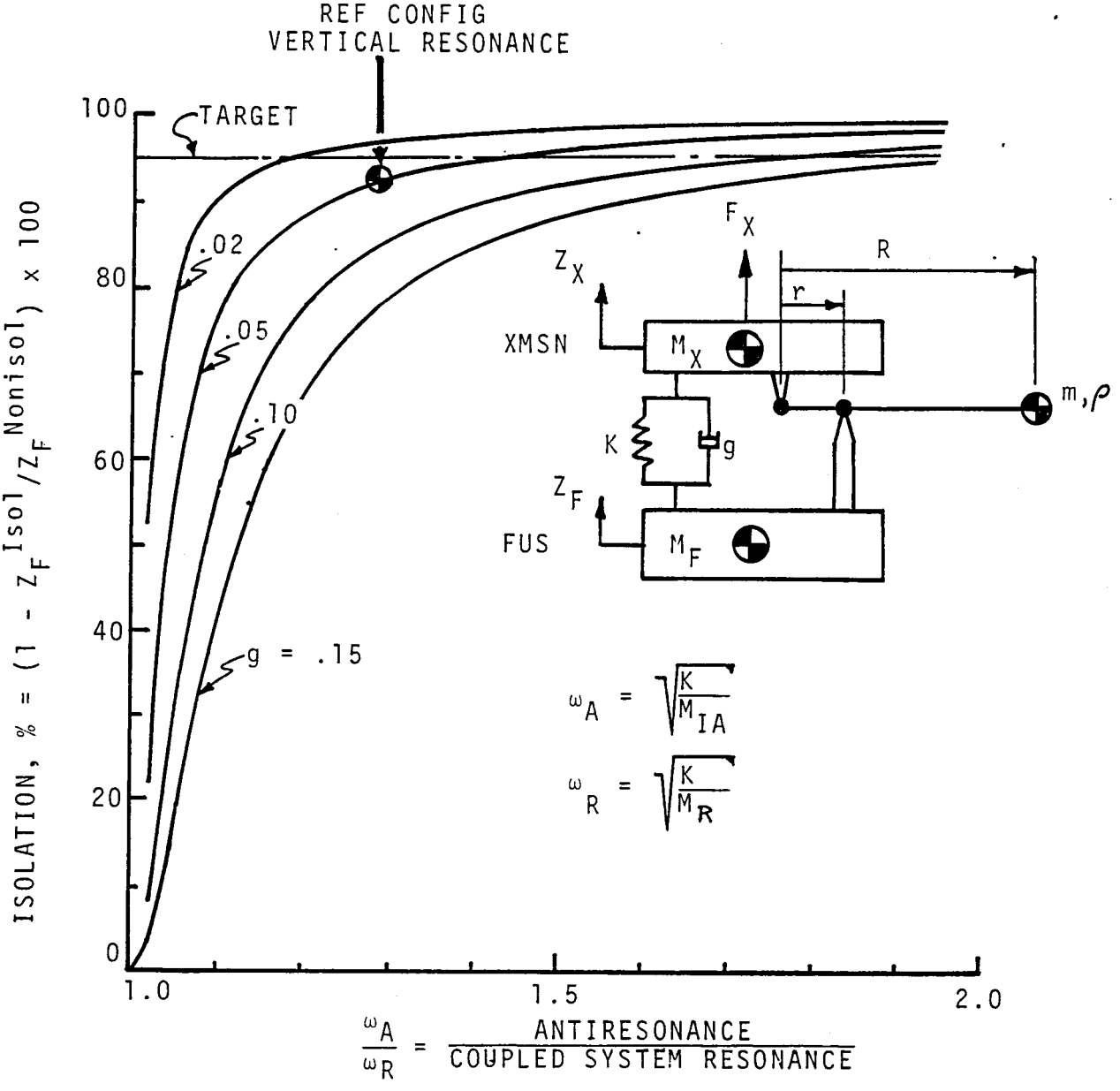

Figure 3.3-11 Damping effect on system isolation efficiency

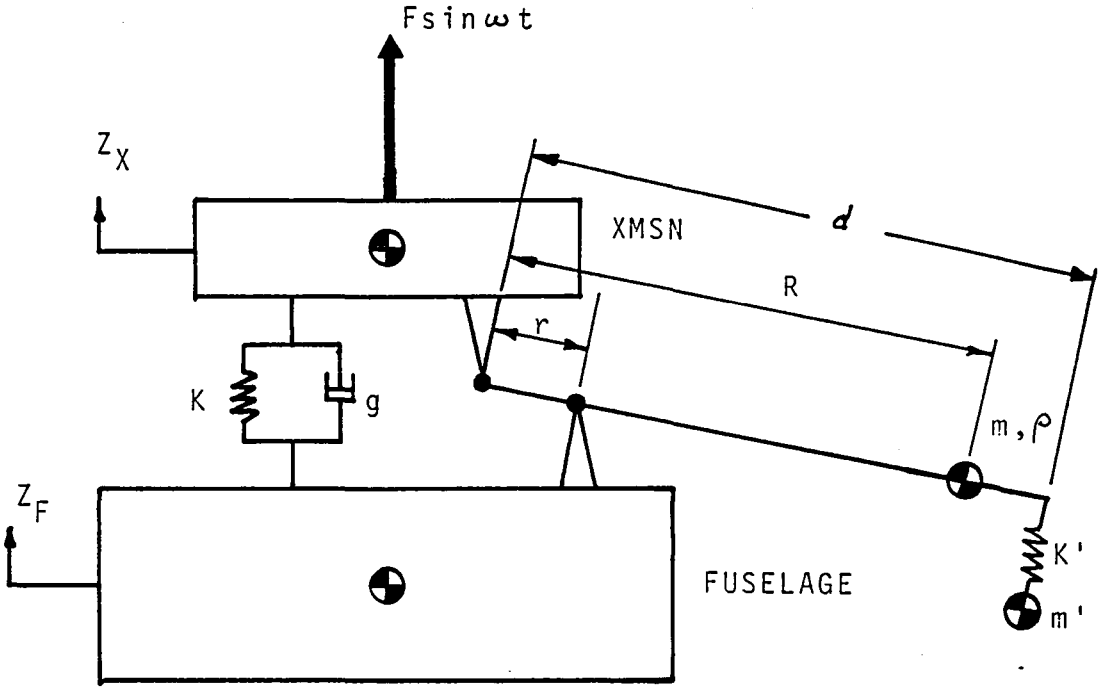

Figure 3.6-1 Dual frequency IRIS schematic

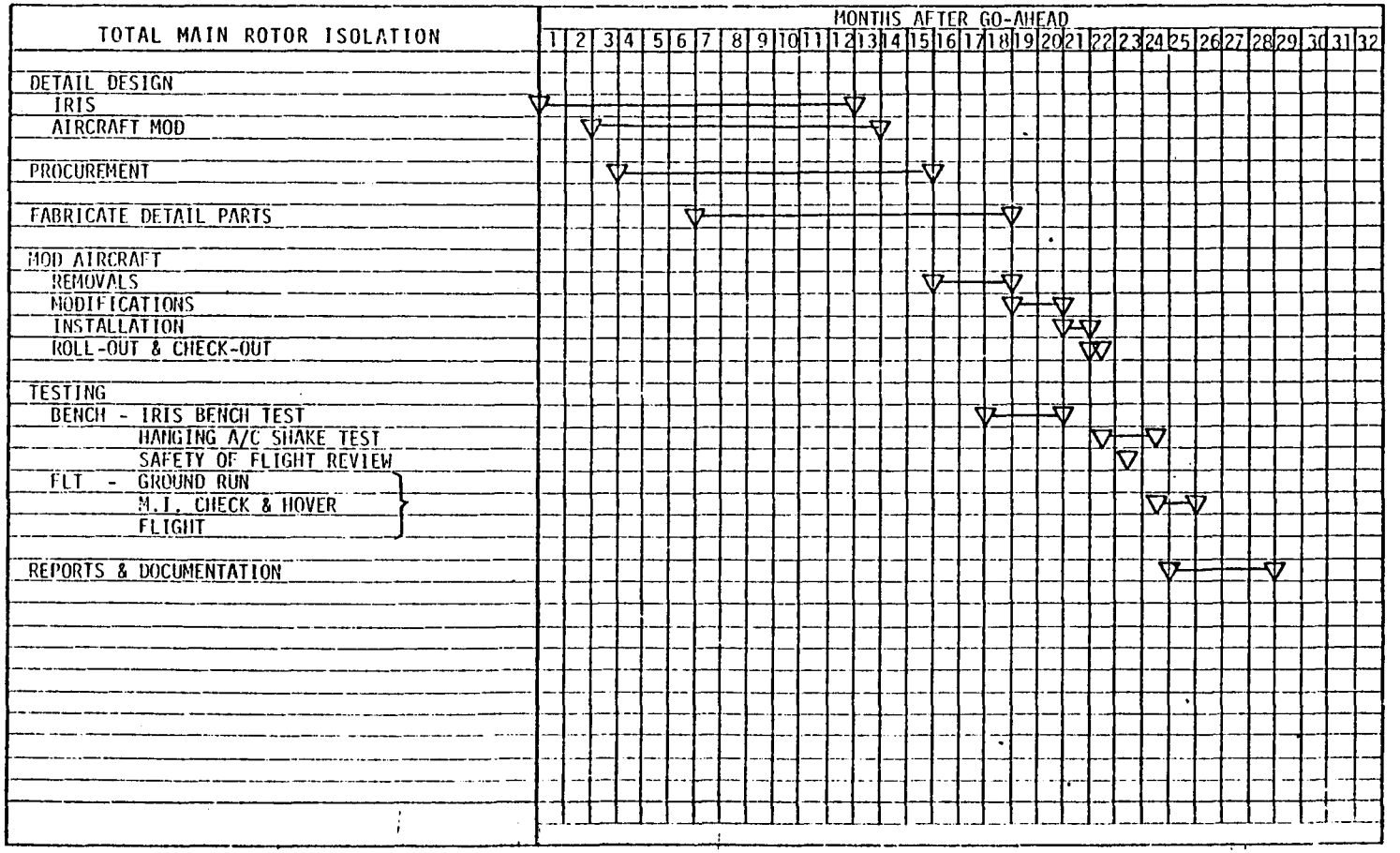

Figure 4-1 Detail design and test schedule

1 Report No	2 Government Accession No	3 Recipient's Catalog No
NASA CR-165666		

4 Title and Subtitle	5 Report Date
TOTAL MAIN ROTOR ISOLATION SYSTEM ANALYSIS	March 1981
	6 Performing Organization Code

7 Author(s)	8 Performing Organization Report No
V. Sankewitsch	D-210-11788-1
	10 Work Unit No

9 Performing Organization Name and Address	11 Contract or Grant No
Boeing Vertol Company Boeing Center P.O. Box 16858 Philadelphia, Pa. 19142	NAS1-16176
	13 Type of Report and Period Covered
12 Sponsoring Agency Name and Address	Contractor Report
National Aeronautics and Space Administration Langley Research Center Hampton, Va. 23665	14 Sponsoring Agency Code

15 Supplementary Notes

Langley technical monitor: Dr. Felton D. Bartlett, Jr.
The contract research effort which has led to the results of this report was financially supported by the Structures Laboratory, USARTL (AVRADCOM).

16 Abstract

This report presents requirements, preliminary design, and verification procedures for a total main rotor isolation system at n/rev. The fuselage is isolated from the vibration-inducing main rotor at one frequency in all degrees of feeedom by four antiresonant isolation units. Effects of parametric variations on isolation system performance are evaluated.

17 Key Words (Suggested by Author(s))	18 Distribution Statement
Rotor isolation Antiresonance Resonance	Unclassified-Unlimited

19 Security Classif (of this report)	20 Security Classif (of this page)	21 No of Pages	22 Price*
Unclassified	Unclassified	74	

End of Document